Cerebral Cortex August 2007;17:1841-1857
doi:10.1093/cercor/bhl093
Advance Access publication October 31, 2006

Attentional Modulation of Receptive Field Structure in Area 7a of the Behaving Monkey

Salma Quraishi[1,2], Barbara Heider[1] and Ralph M. Siegel[1]

[1]Center for Molecular and Behavioral Neuroscience, Rutgers University, 197 University Avenue, Newark, NJ 07102, USA
[2]Current address: Neurological Sciences Institute, Oregon Health & Science University, 505 NW 185th Avenue, Beaverton, OR 97006, USA

Spatial attention modulates the activity of inferior parietal neurons. A statistically rigorous approach to classical retinotopic mapping was used to quantify the receptive fields of area 7a neurons under 2 attentional conditions. Measurements were made with retinal stimulation held constant and the locus of attention manipulated covertly. Both tasks required central fixation but differed in the locus of covert attention (either on the center fixation point or on a peripheral square target in one of 25 locations). The neuron's identity over the recording session was confirmed using chaos theory to characterize unique temporal patterns. Sixty-six percent of the neurons changed prestimulus activity based on task state. Retinotopic mapping showed no evidence for foveal sparing. Attentional factors influenced visual responses for ~30% of the neurons. Two types of modulation were equally observed. One group of cells had a multiplicative scaling of response, with equal instances of enhancement and suppression. A second group of cells had a complex interaction of visual and attentional signals, such that spatial tuning was subject to a nonlinear modulation across the visual field based on attentional constraints. These 2 cell groups may have different roles in the shift of attention preceding motor behaviors and may underlie shifts in parietal retinotopic maps observed with intrinsic optical imaging.

Keywords: attention, chaos theory, cortex, retinotopic map, spatial representation

Introduction

It is well established that attention, both featural and spatial in nature, has pervasive effects on neural responses throughout extrastriate cortex (Moran and Desimone 1985; Maunsell 1995; Desimone and Duncan 1996; Luck et al. 1997; Motter 1998). Damage to parietal regions results in a variety of attentional, visuospatial, and visuomotor deficits in both humans (Bàlint 1909; Bisiach et al. 1986; Karnath et al. 2004) and monkeys (Gaffan and Hornak 1997; Marshall et al. 2002), which are marked by profound hemispatial neglect, coupled with a variety of visuomotor impairments. These symptoms may arise from a faulty central attentional mechanism, leading to an inability to orient toward and select stimuli from a complex visual environment (Lynch et al. 1977; Critchley 1978; Mesulam 1999; Kastner and Ungerleider 2000; Michel and Henaff 2004).

The parietal area 7a is situated at the apex of the parietal stream and is distinct in terms of connectivity as well as functionality from neighboring areas such as lateral, ventral, and anterior intraparietal (LIP, VIP, and AIP, respectively) areas (Gnadt and Andersen 1988; Cavada and Goldman-Rakic 1989; Andersen, Bracewell, et al. 1990; Siegel and Read 1997b; Lewis and Van Essen 2000a, 2000b; Rozzi et al. 2006). Neurons in area 7a provide information about the spatial location of visual cues and combine retinal signals with multiple extraretinal inputs such as orbital eye position and head position (Andersen et al. 1985; Read and Siegel 1997; Siegel et al. 2003). Receptive fields in area 7a are large and generally bilateral (Motter and Mountcastle 1981). Evidence from physiological studies in area 7a have revealed visual properties that are powerfully modulated by overall states of attention (Mountcastle et al. 1981; Goldberg and Bruce 1985; Mountcastle et al. 1987; Steinmetz and Constantinidis 1995). The visual activity of 7a neurons is also influenced by covert shifts of attention away from the point of fixation (Bushnell et al. 1981; Steinmetz et al. 1994; Constantinidis and Steinmetz 2001).

Recent optical imaging studies in behaving monkey have demonstrated three topographic maps across the inferior parietal lobule. The gain field maps represent the eye position signal modulating visual response. Area 7a and nearby dorsal prelunate have lower and upper eye position gain field maps, respectively, which are stable in time (Siegel et al. 2003). The representation of retinotopy and attentional locus are more complex. Retinotopy across area 7a is gradually mapped across the cortical surface; however, it is variable across days and contains bilateral representations (Heider et al. 2005). Attentional locus is mapped as multiple patches within the gain field organization, with shifts of the patch locations across days (Raffi and Siegel 2005). Both ipsilateral and contralateral attentional patches are observed. The shifts in the retinotopic maps and the attentional patches could arise from shifts in receptive field locations that should be observable with electrical measurements under variable task conditions. However, electrophysiological studies conflict as to the direction and degree of modulation, and there is a lack of quantitative analysis of the extent of attentional modulation over the breadth of the visual field.

The aims of the current study were 2-fold. The first aim was to better understand the nature and modulation of the receptive field organization of neurons in area 7a with varying attentional conditions using a variation of Wurtz's elegant saccadic enhancement task (Goldberg and Wurtz 1972). The second aim was to examine whether there were receptive field shifts as predicted from the optical data. This was achieved by recording neural responses with large visual field stimulation while monkeys performed 2 tasks that provided identical retinal stimulation but required 2 distinct attentional rules. The simplest of visual test stimuli (5° squares) were utilized in order to ensure that second-order mechanisms (e.g., local motion selectivity) might not contribute to the receptive field measurements.

Detailed receptive field plots were obtained over a 2- to 4-h recording session under these 2 conditions. It was essential to demonstrate that the changes in receptive field properties over this period were not caused by simply losing isolation of the

neuron. Interspike interval return maps derived from chaos theory (Siegel 1990; Siegel and Read 1993a, 1993b; Ylinen et al. 1995; Read and Siegel 1996; Siegel and Read 2001) were used as a fingerprint of the temporal patterns of activity. This approach demonstrated that the temporal pattern for a neuron did not change throughout the experiment.

A general linear model was used to model the receptive field shape from the neural data. The quadratic model was chosen because of its statistical robustness and well-understood properties. Further, the results are directly comparable to previous electrophysiological (Read and Siegel 1997) and optical studies (Heider et al. 2005). Other models with cylindrical or Gaussian functions could be used; however, the estimation of parameter errors associated with these models is poorly understood, requiring ad hoc approaches for "stepwise" parameter selection.

Two attentional effects were observed across the population of neurons. First, the baseline firing rate differed between the 2 sets of attentional rules. Second, the receptive fields were modulated by locus of attention. A subset of neurons were subject to modulation of neural activity "uniformly" across the visual field in a fashion consistent with the "multiplicative scaling" seen elsewhere in extrastriate cortex due to attentional influence (Connor et al. 1996, 1997; McAdams and Maunsell 1999; Treue and Martinez Trujillo 1999). Another population showed spatially nonuniform effects, which are inconsistent with a purely multiplicative modulation. Parts of this study have been presented previously in abstract form (Quraishi and Siegel 1997a, 1997b).

Methods

Behavioral Task, Visual Stimuli, and Recording

Receptive fields were mapped by measuring neural responses to a 5° stationary white probe square (10 cd/m^2) presented on a black background (1 cd/m^2) at one of 25 locations within a 40° × 40° grid of visual space (Fig. 1*A*). All visual displays were presented on a video monitor (VGA Mitsubishi XC3315C, 83 cm diagonal) placed at a viewing distance of 57 cm from the animal. Eye position was monitored with an infrared eye tracker (ISCAN RK-416, Cambridge, MA) to be within 1° of visual angle.

Prior studies have shown a substantial selectivity for optic flow in area 7a (Siegel and Read 1997a). However, these motion stimuli were not used for a number of reasons. First, attention may be drawn even to a static object when one of its qualities changes. Second, the responses to optic flow and static stimuli are not necessarily similar for area 7a. Third, global optic flow, although a strong stimulus for area 7a, contains local motion components. Although for many area 7a neurons, the response to the global stimulus is independent of local receptive field responses, this is not necessarily true for all area 7a neurons. Using a static test stimulus avoids this confound. Finally, there is a substantial literature on static stimuli, both in area 7a and elsewhere to which the current results can be compared.

For a given trial, a 0.5° red fixation dot appeared in the center of the screen signaling the animal to pull a lever and to start fixating for the duration of the trial. Following a 2-s delay, the square stimulus appeared in one of the 25 positions (5 × 5 grid). The animal performed 2 types of task that were presented in separate behavioral blocks. The block name indicates the particular visual stimulus that was attended during each block. In the "FIX" block, the animal released the lever in response to the dimming of the fixation dot at a random time from 1500 to 4000 ms (1500–3500 ms for monkey F) following stimulus onset (Fig. 1*B*). In the "PROBE" block, the animal responded to the dimming of the target (probe) stimulus (2 cd/m^2) at a random time within the same interval, while the monkey's eyes remained fixed in the primary central position (Fig. 1*C*). Trials were presented in a fixed random block design such that the animal could not predict the location of the upcoming square within a block. ("Fixed random block" means the monkey has to get one of each condition correct before proceeding to the next group of trials.) In addition, FIX and PROBE trial types were never mixed within a particular behavioral block, so the monkey knew specifically where to allocate attention within a block of trials. Typically, the PROBE block was performed first, followed immediately by the FIX block (101 experiments). In 11 experiments, the order was reversed. No systematic effect of the order of presentation on performance was observed.

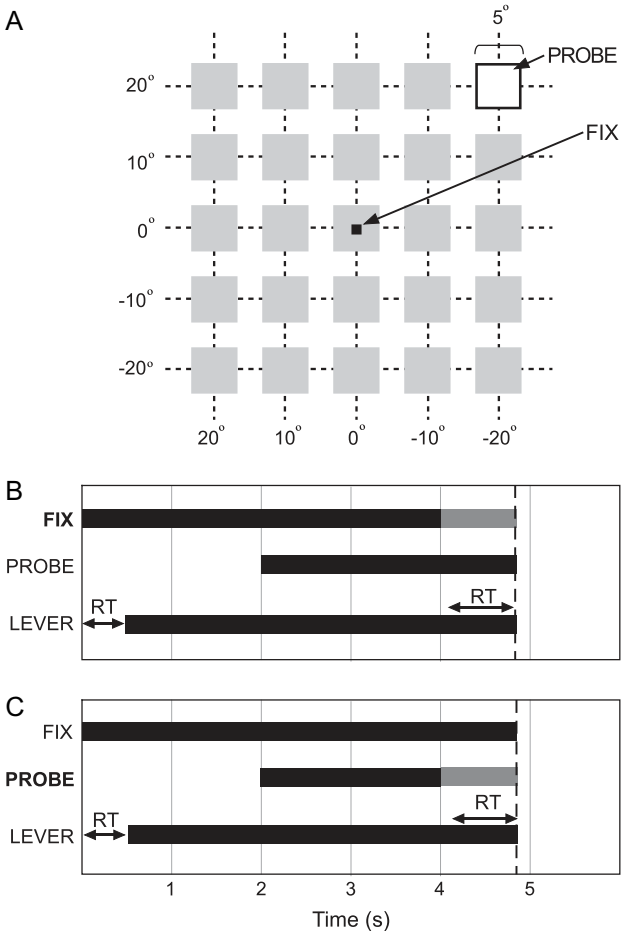

Figure 1. Spatial array of the 25 locations tested during receptive field mapping (*A*) and temporal sequence of the behavioral task for one trial of each task type, FIX (*B*) and PROBE (*C*). In both trial types, the fixation target appears at time 0 ms, and the animal is required to pull back the lever within 400 ms to initiate the trial. A probe stimulus appears 2000 ms later. (*B*) During FIX trials, the fixation target dimmed at a random time between 3500 and 6000 ms (3500–5500 ms for monkey F) into the trial (indicated in this Figure at 4500 ms, gray bar). (*C*) In PROBE trials, the probe stimulus dimmed at some point during the same interval (indicated again at 4500 ms, gray bar). The animal was required to release the lever within 800 ms after the dimming to receive a juice reward. RT, reaction time.

Extracellular single-unit recordings were made using glass-coated, platinum–iridium electrodes of 1–5 MΩ impedance at 1 KHz as described elsewhere (Siegel and Read 1997a) with interspike intervals measured with a 0.1-ms precision (Ratzlaff and Siegel 1990). Extreme care was taken to monitor the cell's action potential shape throughout the 2-h experiment to ensure stability and stationarity in the recordings; if the unit shape merged with a second unit or was ambiguous, then the experiment was eliminated. In practice this happened only 2 times. Recordings were made from 106 area 7a neurons taken from one left hemisphere of one animal and one right hemisphere of another animal.

Statistical Analyses

Comparison of Prestimulus Baseline Activity

Baseline activity was defined as a neuron's activity in the 500-ms interval prior to probe onset (prestimulus period). All parameters, including

visual stimulation, lever state, and eye position were identical for both behavioral blocks during this measurement interval. Baseline firing rates during FIX trials were compared with those found during PROBE trials for each neuron (paired, 2-tailed *t*-test, $P < 0.05$). A contrast ratio was computed to quantify the effect of task on baseline activity, $CR = (b_p - b_f)/(b_p + b_f)$, where b_p is the average of the basal firing rate during PROBE trials and b_f is the average of the basal firing rate during FIX trials. Index values occurred in a bounded range between –1 and 1, with positive values indicating cells with higher basal firing rate during PROBE trials and negative values indicating cells with higher basal firing rate during FIX trials.

Determination of Visual Responsiveness

Neurons were first analyzed if they responded to the visual stimulus for at least one of the 25 mapping positions, in either behavioral block. Visual responsiveness was determined statistically via a 2-way analysis of variance (ANOVA) performed on the neuron's response within each block of behavioral trials (Siegel and Read 1997a). The dependent variable was neural firing rate, and the first independent factor corresponded to each of the mapping positions (25 levels). The second factor provided a categorical code that denoted the time period of the firing activity (before vs. after stimulus onset). It is important to note that this step of the analysis makes no assumptions as to the receptive field shape of the neuron. It simply asks whether a change in firing rate is significantly dependent on the position of the stimulus.

All firing rates were computed over 500 ms, and the significance level for all analyses was set at $P < 0.05$. Data from each block were analyzed separately. A data set with an effect of time period, either alone (TYPE 1) or as an interaction with spatial position (TYPE 2) was defined as visual, and the cell was further analyzed. Cells that had no significant effect of time period in both FIX and PROBE blocks (TYPE 0) were considered nonvisual and were not considered further.

Comparisons of Receptive Field Structure

To separate spatial versus nonspatial receptive fields and block effects, a second 2-way ANOVA was computed, in which the dependent variable was the change in firing rate at stimulus onset, computed as the difference between prestimulus baseline firing rate and the evoked firing rate starting at stimulus onset. The first independent factor was block type (BLOCK factor, 2 levels, FIX or PROBE), and the second factor corresponded to each of the 25 mapping positions (POS factor, 25 levels). Significance was set at $P < 0.05$. A similar method was adapted for the analysis of behavioral reaction times (see Results).

Various combinations of effects are possible. A cell with a significant effect of spatial position (POS) is defined as having a spatially selective receptive field. A cell with a significant effect of block type (BLOCK) is modulated by the task. An effect of POS alone indicates a cell with a receptive field structure but no effect of the task. If the BLOCK effect is found alone, the cell shows a uniform (nonspatially tuned) response, and the firing rates are modulated in toto from one block to the next. Combined effects of BLOCK and POS indicate a cell that is spatially selective; however, the firing rate is modulated *in toto*, such that the spatial selectivity is maintained across blocks, and manifests as a "gain" change of firing rate. Finally, an interaction of the main effects (BLOCK × POS) indicates a change in spatial selectivity across blocks. Table 1 outlines the statistical results of this analysis and the classification scheme used to identify subgroups within the population. A 2-part notation was adopted to refer to each cell's combination of effects; the first character designates the absence or presence of a task effect (∅ or G, respectively) and the second denotes the absence or presence of spatial selectivity (∅ or Sp, respectively).

Receptive Field Shape Analysis by Regression Models

Quadratic models were used to characterize the dependence of evoked activity upon retinal position of the stimulus for all spatially selective cells. Spatially selective cells are defined to have a significant effect of POS, either combined with a BLOCK effect (GSp), or singly (∅Sp), or in form of an interaction of these main effects (G × Sp). The combination of significant dependent variables in the ANOVA determined the model that was used to fit the physiological data (Table 1).

Cells that had no effect of BLOCK in the prior analysis (∅Sp) were analyzed by merging data from both behavioral blocks (FIX and PROBE). The dependent measure was the neuron's firing rate during the first 500 ms of stimulus presentation. A surface was fit by regression using the following general model:

$$A_i(X, Y) = a_x X + a_y Y + a_{xx} X^2 + a_{yy} Y^2 + a_{xy} XY + b + \mathcal{E}_i, \qquad (1)$$

where "A_i" is the ith measurement of the change in rate from baseline, "X" and "Y" describe the horizontal and vertical coordinates of the stimulus and "a_x" and "a_y" are the coefficients for horizontal and vertical dimensions. Quadratic terms are "a_{xx}" and "a_{yy}," and "a_{xy}" is a horizontal–vertical interaction term. The neuron's firing rate for foveal stimuli at (0°, 0°) is given by "b," and "$\mathcal{E}_i$" is the residual error reflecting the difference between the predicted and actual measurement of the ith value. The a and b parameters were fit using linear regression by a stepwise procedure to introduce and remove variables at the $P = 0.05$ level (GLM Procedure, SAS Co., Durham, NC).

A different model was used for comparison of physiological data with respect to block type for cells that had an effect of block alone (G∅). These cells had a uniform firing rate for all spatial positions within a block but different mean firing rates across blocks. The mean firing rates within block were modeled separately using the following equation:

$$A_i(X, Y) = (p_b + Tf_b) + \mathcal{E}_i. \qquad (2)$$

This formulation is equivalent to a 1-way ANOVA in which the mean firing rate for FIX surfaces is given by the value $(p_b + Tf_b)$, where T is a categorical coding variable and can be interpreted as having a value of "1" for all FIX trials and "0" for all PROBE trials. The Tf_b term drops out for PROBE firing rates, where $T = 0$, leaving the PROBE mean firing rate equal to the coefficient p_b.

In instances of multiple main effects or an interaction of main effects, 2 additional models were used. These were cells that had an effect of

Table 1
Classification of receptive field modulations

Block	Position	Interaction	Gain	Spatial	TYPE	MODEL
−−−	−−−	−−−	−−−	−−−	ØØ	NA
−−−	+++	−−−	−−−	Yes	ØSp	$A_i(X, Y) = a_x X_i + a_y Y_i + a_{xx} X_i^2 + a_{yy} Y_i^2 + a_{xy} XY + b + \varepsilon_i$
+++	−−−	−−−	Yes	−−−	GØ	$A_i(X, Y) = (p_b + Tf_b) + \varepsilon_i$
+++	+++	−−−	Yes	Yes	GSp	$A_i(X, Y) = a_x X_i + a_y Y_i + a_{xx} X_i^2 + a_{yy} Y_i^2 + a_{xy} XY + (p_b + Tf_b) + \varepsilon_i$
Either	Either	+++	NA	Yes	GxSp	$A_i(X, Y) = (p_x + Tf_x) X_i + (p_y + Tf_y) Y_i + (p_{xx} + Tf_{xx}) X_i^2 + (p_{yy} + Tf_{yy}) Y_i^2 + (p_{xy} + Tf_{xy}) XY + (p_b + Tf_b) + \varepsilon_i$

Note: Cells with no main effects or an interaction were classified as nonmodulated, nonspatial, or "ØØ", indicating that their visually evoked responses did not change depending on task nor were they spatially selective. Another group of cells that remained unchanged by task were spatially selective and statistically the same across task blocks (nonmodulated, spatial, or ØSp). All remaining cells were modulated by task requirement in some fashion. Those that had a significant effect of block alone were classified gain, nonspatial (GØ). These cells had a constant (i.e., nonspatial) response across the area of visual field tested, which changed in amplitude or gain according to task. Another group of gain-modulated cells had spatial receptive fields that remained the same across tasks, but with an overall change in firing rate amplitude across the visual field (gain-spatial, GSp). A final group of cells (G × Sp) showed an interaction of the 2 independent factors, indicating that these cells had more complex spatial changes in receptive field across task. All spatially selective cells (ØSp, GSp, and G × Sp) were subsequently characterized using the quadratic methods described in the Methods. ØØ and ØSp are nonmodulated subclasses; GØ, GSp, and GxSp are modulated. +++ Indicates $P < 0.05$ or significant effect.

POS combined with an effect of BLOCK (GSp) or an interaction of main effects (G × Sp). GSp cells were analyzed using a combination of equations (1) and (2). This was essentially the same general linear model as above, with an additional term that provided a categorical code denoting block type included only in the model intercept. The result was a model that allowed for a spatially complex fit of the data and 2 resulting intercept values coded by block that described the amplitude by which the modeled receptive field shifted according to task block. For these cases, both blocks of firing rate data from a single cell were taken together and coded with respect to block type. Firing rates were modeled along the horizontal and vertical dimensions as above; however, this version of the model contained an additional term "T" in the intercept value, either the binary value "0" or "1" based on block type (FIX or PROBE):

$$A_i(X, Y) = a_x X + a_Y Y + a_{xx} X^2 + a_{yy} Y^2 + a_{xy} XY + (p_b + Tf_b) + \mathcal{E}_i. \quad (3)$$

The "p_b" term is a coefficient that provides the intercept value for the PROBE data, that is, in instances that the "T" term is equal to "0." For "T" values of "1," an "f_b" component is generated, which when added to the "p_b" term gives the intercept value for the FIX surface. It should be noted that the dependence of the firing rate on position for FIX and PROBE data is identical in this model, with the only difference in the 2 surfaces being a change in intercept value.

The third and final model was used in cases where cells had a significant "interaction" of BLOCK and POS (G × Sp) in the ANOVA above. These cells had a different pattern of spatial responses in FIX versus PROBE blocks. A stepwise regression was performed; however, the model here includes the variable "T" for task type (i.e., FIX vs. PROBE) associated with all the regression coefficients, in addition to the intercept term:

$$\begin{aligned} A_i(X, Y) = {} & (p_x + Tf_x) X_i + (p_y + Tf_y) Y_i + (p_{xx} + Tf_{xx}) X_i^2 \\ & + (p_{yy} + Tf_{yy}) Y_i^2 + (p_{xy} + Tf_{xy}) X_i Y_i + (p_b + Tf_b) + \mathcal{E}_i. \end{aligned} \quad (4)$$

According to this model, coefficients that determine the surface contour for trials in the PROBE block are determined by "p" parameters, and "f" parameters are terms that describe how the surface changes in the FIX condition. Again, the categorical variable "T" takes the binary value of either "0" or "1" based on whether the data entered is from the FIX or PROBE block. Linear regression by stepwise selection is used to fit "p" and "f" parameters by introducing and removing variables at the $P = 0.05$ level. If all "f" parameters are 0, then both task types yield the same contour receptive field. If any "f" parameters are significant, then 2 spatially different receptive field shapes result from the 2 data sets.

A stepwise selection procedure was used in all fits in order to circumvent the problem of specious error propagation into the estimated coefficients that is often associated with standard regression techniques (Read and Siegel 1997). A test of significance is done for every term that is entered or removed from the final model. If entry of a new term into the model renders a preexisting term nonsignificant, the preexisting term is then removed from the final model. Use of the stepwise function ensures that additional parameters that have no statistical basis will not be estimated, which prevents the final model being overdetermined. Typically between 2 and 4 iterations occur to yield a final model, which contains an intercept and 2 to 4 significant terms having P values of about 0.001. Thus, a final fit might consist of just 3 parameters: a_x, a_{yy}, and b (i.e., $A(x, y) = a_{yy} Y^2 + a_x X + b + \mathcal{E}_i$).

The dimensions of the resulting receptive fields were analyzed by examining the combination of significant parameters yielded for each neuron and their coefficients of fit. Cells that had a quadratic dependence along both the horizontal and vertical had either a local maximum ("peak," negative a_{xx} and a_{yy} terms) or minimum response ("trough," positive a_{xx} and a_{yy} terms) located in the visual field (Heider et al. 2005). The center of each receptive field was defined as the visual field location at which the neuron's critical value (i.e., maximum or minimum firing rate) occurred. Cells with quadratic dependence along both axes without additional linear dependence had a critical value occurring at the fovea (0°, 0°). Cells that had the addition of a linear term were shifted to a location defined by the coordinates (X_c, Y_c), where, $X_c = -a_x/2a_{xx}$ and $Y_c = -a_y/2a_{yy}$. Cells that were fit with a negative quadratic term (peaked receptive fields) in the horizontal had 2 visual field locations at which the firing rate was 50% of the critical value, given by:

$$2\frac{-a_x + \sqrt{\frac{a_x^2 - 4a_{xx}b}{2a_{xx}}}}{2a_{xx}} \text{ and } 2\frac{-a_x - \sqrt{\frac{a_x^2 - 4a_{xx}b}{2a_{xx}}}}{2a_{xx}},$$

where the quantities a_x and a_{xx} are interchangeable with a_y and a_{yy} for cells with dependencies along only the vertical. The difference of these 2 values represents the receptive field width at half-height and provides a descriptive marker for receptive field dimension (Anderson and Siegel 1999).

Interspike Interval Return Maps

Interspike interval return maps show unique configurations dependent on the temporal patterns of activity of a neuron (Siegel 1990; Siegel and Read 1993a, 1993b; Ylinen et al. 1995; Read and Siegel 1996). They are derived from chaos theory and a particular theorem by Takens (1981) that states the nonlinear dynamics of a system can be derived from phase-lagged data. Although the interspike interval return maps do not exactly satisfy the requirements of Takens' theorem making it impossible to completely reconstruct the underlying dynamical system (Siegel and Read 2001), they do encapsulate the temporal dynamics of single neurons.

In the current study, the goal was not so much to explore the range of dynamics but rather to confirm the identity of a neuron throughout a recording period. Interspike interval return maps were constructed for all correct trials for each pair of experimental runs (FIX vs. PROBE). They are created by plotting the points ISI($i + 1$), ISI(i), where ISI(i) is the ith interspike interval. Logarithmic (base 10) axes were utilized to assist in viewing wide dynamic range of a neuron from 0.1 to 10 000 ms.

The similarity of the 2 interspike interval return maps for the FIX and PROBE conditions were compared by converting each of the return maps to 2-dimensional density plots $\Psi(I,J)/N$, where N is the number of spikes. $\Psi(I,J)$ essentially was a 2-dimensional histogram constructed with a 51 × 51 grid in the space of (−1, 3) log units for both the ISI(k) and ISI($k + 1$) axes; each density plot $\Psi_{\mathrm{FIX}}(I,J)$ and $\Psi_{\mathrm{PROBE}}(I,J)$ was normalized by the total number of spikes (N_{FIX} and N_{PROBE}). The root mean square (RMS) error between the FIX and PROBE density plots was used as a similarity measure of the RMS error: $\Xi = \sqrt{\sum_{I,J=1}^{51} \{\psi_{\mathrm{FIX}}(I,J) - \psi_{\mathrm{PROBE}}(I,J)\}^2}$. If the RMS error ($\Xi$) was very small, this indicated that the 2 density plots and the 2 interspike interval return maps were similar. This was evidence that the same temporal pattern and, by extension, the same neuron were recorded under both conditions. A large RMS error could indicate one of two possibilities: either the neuron had changed its temporal firing pattern (i.e., indicating loss of, or change in, the isolation of the neuron) or that there was a substantial change in firing rate between the 2 conditions.

In order to determine a probability distribution for Ξ, all possible pairing between sessions were made. Thus, a single FIX block for a particular cell was compared with all FIX and all PROBE blocks for every cell; the same was done for every PROBE block. This created a distribution of 22 262 Ξ calculations. As noted in the Results, these distributions were used to probabilistically examine the validity of a match between the FIX and PROBE runs.

Surgical Procedures

This study was performed in 2 hemispheres of 2 adult male *Macaca mulatta* (4–5 kg, monkeys F, left, and S, right). All surgical procedures were performed aseptically and under general anesthesia as described elsewhere (Siegel and Read 1997a). In brief, a recording chamber was implanted and a 16-mm-diameter craniotomy was made at stereotaxic coordinates derived from structural magnetic resonance image (MRI) scans. Area 7a was localized as the region bounded by the inferior parietal sulcus and the superior temporal sulcus posterior to the Sylvian fissure. Following a 4-day recovery period, standard electrophysiological techniques were used on a daily basis to record neural responses from the cortical surface (within 2 mm from top of neural activity) for up to 1 year. In one animal (monkey S), anatomical location of the recordings was confirmed in the right hemisphere after perfusion, and in the other animal, anatomical location is based on structural MRI. All procedures were performed in accordance with National Institutes of Health

Guidelines for the Care and Use of Laboratory Animals and were approved by the Rutgers University Animal Institutional Review Board.

Results

Behavioral Modulation by Task

Overall, both animals' performance was 95% or above for both FIX and PROBE blocks. If the monkey used different strategies in the FIX versus PROBE blocks, then reaction times should also vary by task type. Thus, reaction times were analyzed using a 2-factor ANOVA that tested the hypothesis of reaction times being dependent on stimulus position and block type. A main effect of block (GØ, GSp) or an interaction (G × Sp) indicates that reaction times varied across blocks (see Methods and Table 1).

A total of 52 sets or pairs (FIX vs. PROBE) of behavioral data (25 from monkey S and 27 from monkey F) were collected. Overall, 36 sets (69%) had a significant effect of block type on the animals' reaction times (Fig. 2*A*), either singly, or combined with position, or as an interaction (GØ, GSp, G × Sp). For every pair of runs the mean was plotted (Fig. 2*B*). In 33 of the 36 significant pairs, the reaction time was longer for the PROBE condition. Fifteen of the remaining 16 pairs showed no effect of parameter (ØØ). This means that both conditions had the same reaction time at all locations under both conditions. One pair had an effect of position independent of block type (ØSp). These latter 2 effects represent experimental sessions in which reaction times were comparable across block and appear to be the result of improved performance due to practice. Overall, both animals showed comparable behavioral results.

To analyze the effects of eccentricity, the reaction time data were regressed upon the stimulus position for 100 runs (50 pairs). In 21 runs (21%), a positive value for the quadratic components (either a_{xx} or a_{yy}) was found indicating an increase of reaction times with eccentricity. Only 7 runs yielded negative quadratic components.

These measures indicate that the dependence of the reaction time upon position was different for the 2 behavioral blocks and that the PROBE task required longer reaction times.

Dependence of Baseline Firing Rate on Behavioral Task

Of the 106 cells which form the database for this study, 70 (66%) had baseline firing rates that differed between FIX and PROBE blocks even though visual stimulation during this time period was identical (i.e., only a center fixation point). A similar proportion of cells showed higher baseline firing rates during the FIX condition as during the PROBE condition, thus there was no systematic effect of block. Half of the 70 neurons responded with higher firing rate during FIX condition. This is evident when plotting baseline firing rates of PROBE against FIX for each of the 70 neurons that had an effect of block type (Fig. 3*A*). The histogram with the contrast index (see Methods) in Figure 3*B* demonstrates the similar distribution of cells showing different firing rates during either behavioral condition.

Dependence of Visual Response on Behavioral Task

Of the 106 cells, 58 (55%) responded differentially to the onset of at least one of the 25 mapping positions, in one or both behavioral blocks (FIX and/or PROBE; Fig. 4). The remaining 48 neurons were not differentially responsive to the onset of the mapping stimulus. These 48 cells were further examined to determine if they responded significantly from baseline but

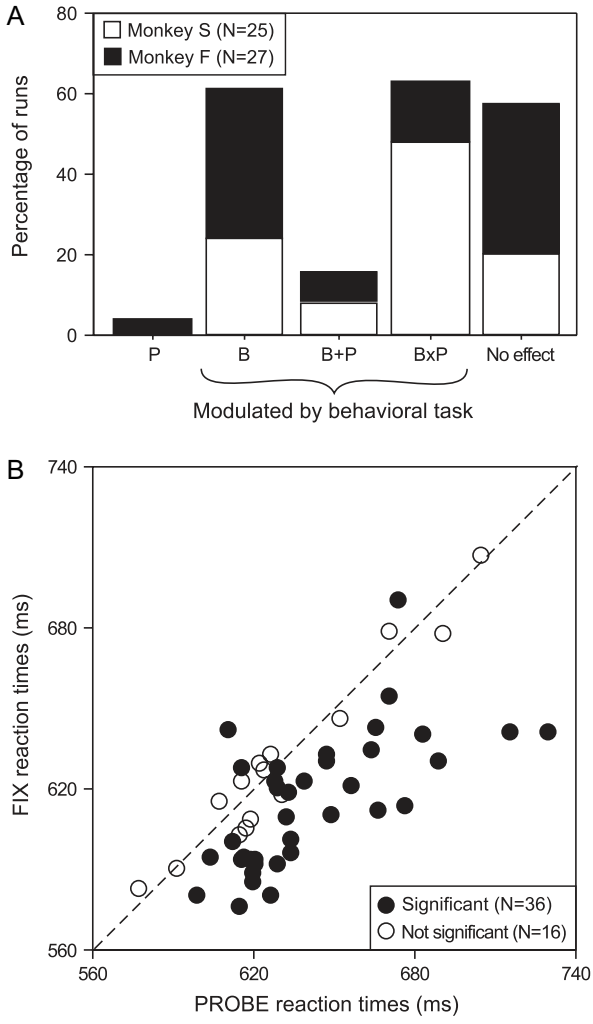

Figure 2. Categories of effects resulting from the 2-way ANOVA (BLOCK × POS) for behavioral data. (*A*) Reaction times were analyzed depending on block (B) and stimulus position (P) separately for the 2 monkeys. Significant results in the B category consisted of a single effect of task (block) type but no effect of position of the target. Significant results in the P category had a single effect of stimulus position but no variations across blocks. Dual additive (B + P) or multiplicative (B × P) effects suggest an interaction based on a combination of the 2 factors. (*B*) Mean reaction times are plotted for each pair of runs (FIX vs. PROBE) separately for pairs with significant block effects (filled circles) and pairs without significant block effects (open circles). Most data points fall below unity line (dashed line).

equally at all positions. A 2-way ANOVA was used to determine if these neurons had visual responses that were independent of stimulus position (i.e., TYPE 1 cells after Siegel and Read 1997). A total of 18 neurons were found to be visually responsive but their response was equal at all positions indicating that their receptive fields were greater than the 40° × 40° region tested (see Fig. 1*A*). Thus, visually responsive neurons were a total of 76 (58 spatially tuned, 18 not spatially tuned) neurons. The remaining 30 unresponsive neurons are not considered further.

The 76 visual neurons were classified based on responses during the 2 behavioral blocks using the 2-way ANOVA with the mapping stimulus position (POS) and behavioral block (BLOCK) as independent measures (see Methods and Table 1). Figure 4 shows the distribution of neuron types observed. Forty percent of the visual cells (30/76) were modulated in some way by the behavioral block, and 37% (28/76) were modulated by the position of the visual stimulus.

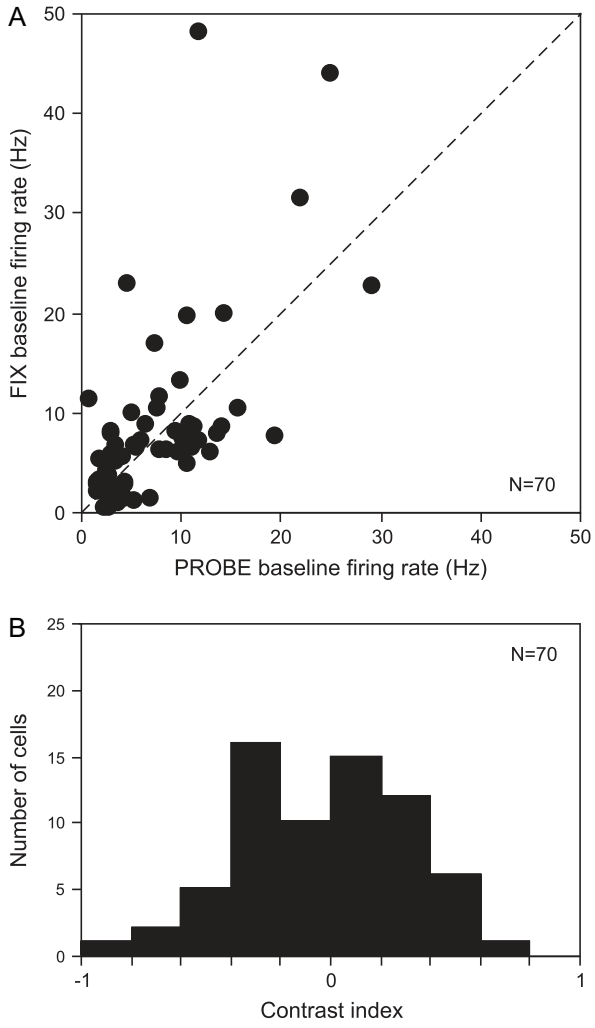

Figure 3. Comparison of average firing rates and modulation indices for FIX versus PROBE baseline activity. (*A*) Baseline firing rates averaged over 8 trial repetitions for FIX trials plotted against a similar value for PROBE trials. Dashed line indicates unity line. (*B*) Distribution of baseline rate modulation indices (contrast index). Indices reflect the difference of average baseline firing rates during FIX and PROBE trials, divided by their sum. Positive values describe cells that have higher baseline firing rates in PROBE trials, and negative values are given to cells that have higher baseline firing rate in FIX trials.

Comparison of Baseline Firing Rate and Visual Response

It would be expected that if common mechanisms were responsible for both the baseline and visual modulation by block, there should be a correlation between the 2 effects. Under this assumption, a majority of neurons would have a significant baseline modulation in conjunction with a visual modulation. The null hypothesis is that there is no relationship between the 2 effects. The distribution of effects from the ANOVA was determined by comparing whether baseline or visually evoked activity was dependent on the block (FIX vs. PROBE). A χ^2 test did not reach significance, and thus it was not found to deviate from the null hypothesis. This suggests that the mechanism responsible for the baseline effect is different from that responsible for the visual modulation.

Task-Independent Neurons

A total of 60% (46/76) of the visually responsive neurons did not show task-related modulation (i.e., they responded invariantly

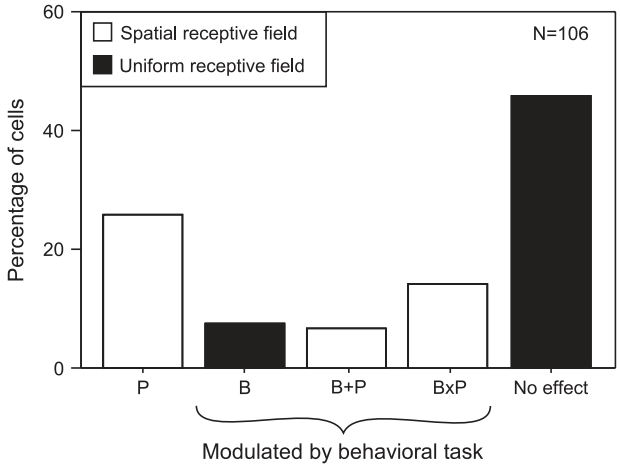

Figure 4. Categories of effects resulting from the 2-way ANOVA (BLOCK × POS) are plotted physiological data. Firing rates were analyzed depending on block (B) and stimulus position (P). Significant results in the B category consisted of a single effect of task (block) type but no effect of position of the target. Neurons with this response pattern were categorized as GØ cells. Significant results in the P category had a single effect of stimulus position but no variations across blocks. Neurons in this class were labeled ØSp cells. Dual additive (B + P) or multiplicative (B × P) effects suggest a complex difference based on a combination of the 2 factors (GSp and G × Sp cells, respectively).

across blocks). The receptive field properties of this population (28 ØS and 18 ØØ; Table 1) were characterized.

For the 28 cells whose firing rate depended on the stimulus location (ØS), the receptive field surfaces were further characterized using a second-order regression model (eq. 1), which significantly fit 27 ØSp neurons. With the stepwise regression, only significant linear and quadratic components remained in the model. Three of those 27 neurons (11%) were fit solely with linear components, and 24 neurons had at least one significant quadratic term. The presence of quadratic terms in the population reflects the presence of local minima or maxima in the response field.

Task-Dependent Neurons

In 40% (30/76) of the visual cells, the neural response was dependent on the behavioral block with 2 main effects. About half of the cells showed a gain-like effect of the behavioral block with the receptive field shape unchanged (8 GØ, 7 GSp). For 15 G × Sp neurons, the shape of the receptive field was altered by the behavioral task. (These cells were termed G × Sp to indicate the interaction between the 2 effects.)

G Ø Neurons

These 8 neurons had receptive fields that were not spatially selective but the responses were altered by the task condition. The receptive fields may have extended beyond the tested region in some instances. The change in firing rate for the 8 GØ neurons was quantified by grouping the mean firing rates for all positions within a block. A standard index was computed, and no bias for inhibitory or excitatory modulation was observed in the 2 behavioral blocks (not shown).

GSp Neurons

These 7 neurons had receptive field structures modulated by a linearly separable positional dependence and by task block (Fig. 5). Hence, 2 regression surfaces were obtained separated

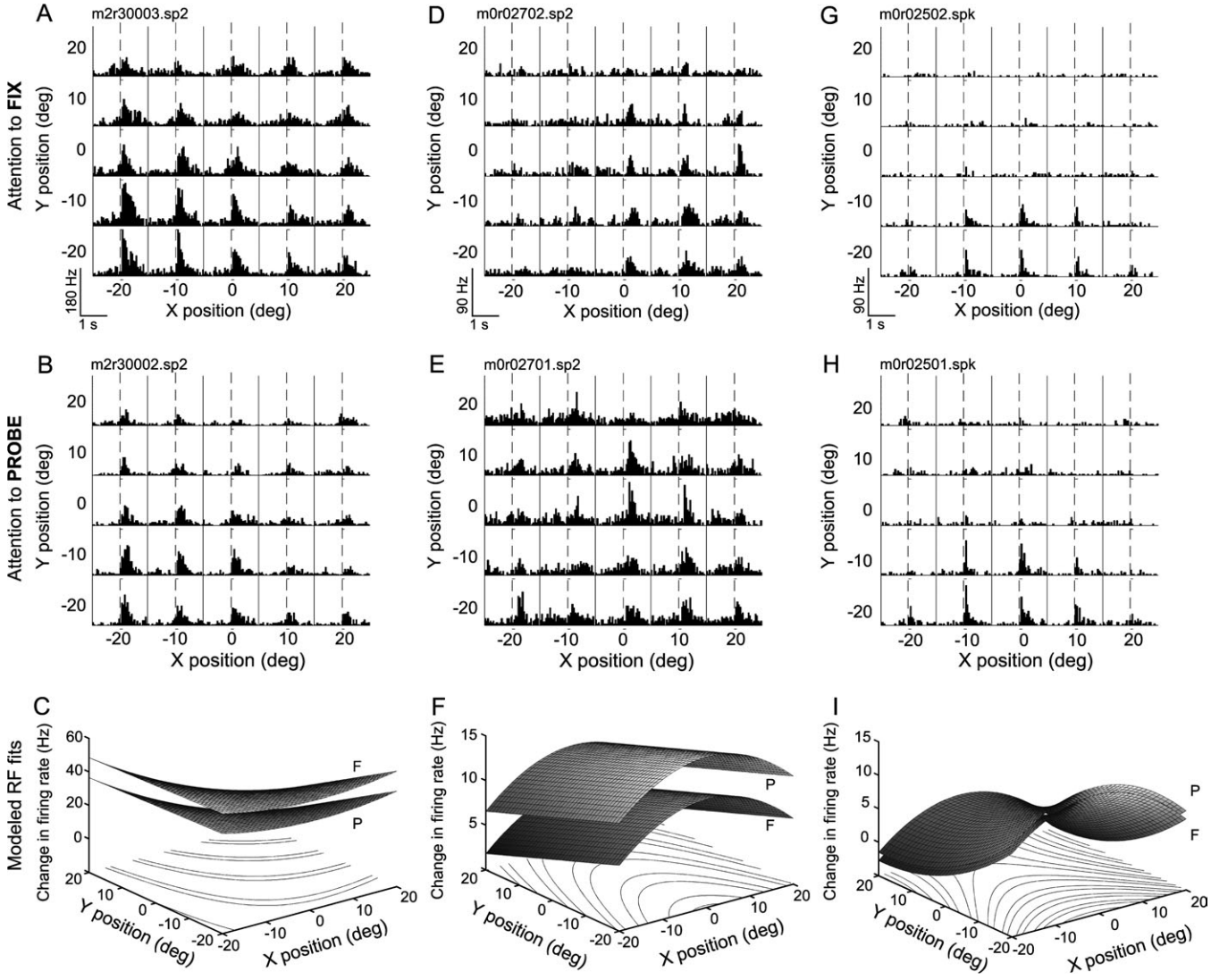

Figure 5. Peristimulus time histograms (PSTHs) and corresponding quantitative fits for 3 representative GSp cells with multiplicative gain modulation of spatial receptive fields. Upper panels (*A*, *D*, *G*) depict neural responses during FIX trials, center panels (*B*, *E*, *H*) depict responses during PROBE trials, and lower panels (*C*, *F*, *I*) show the quantitative surface fits representing each of the above data arrays (F, FIX, and P, PROBE) plotted on a single set of axis. PSTHs represent the cell's mean response over 8 trials for each visual field position. The location of each histogram indicates the location of the stimulus to which those responses correspond (5 × 5 matrix). Dashed lines indicate the onset of the stimulus to which the neural activity is synchronized. (*A*) During FIX trials, neuron is spatially tuned for stimuli appearing in the lower left visual field (−20°, −20°). Regression parameters: $A_{FIX} = -0.645x + 0.656y + 0.014x^2 - 0.029xy + 31.6$. (*B*) The same neuron's evoked response is scaled down, as is the baseline firing rate in PROBE trials. $A_{PROBE} = -0.645x + 0.656y + 0.014x^2 - 0.029xy + 19.69$. (C) The modeled response field of data in (*A*, *B*) reflects this change by the different intercepts. (*D–F*) A neuron that is selective for stimuli appearing in the lower central visual field during both tasks. $A_{FIX} = 0.139y + 0.012x^2 + 9.37$; $A_{PROBE} = 0.139y + 0.012x^2 + 14.1$. Receptive field configuration is identical in FIX and PROBE trials but has evoked responses that are scaled down during FIX trials as compared with PROBE as evident by the smaller intercept. No effect on baseline activity is seen for this cell. (*G*, *H*) A third neuron shows a multiplicative scaling of spatial tuning, this time with increased evoked and baseline responses during PROBE trials. $A_{FIX} = -0.047x + 0.255y - 0.015x^2 + 0.007y^2 + 4.89$; $A_{PROBE} = -0.047x + 0.255y - 0.015x^2 + 0.007y^2 + 6.12$.

by a fixed intercept between the 2 blocks (eq. 3). For example, the neuron in Figure 5*A*,*B* responds preferentially to stimuli appearing in the lower left quadrant (–20°, –20°), as illustrated by the modeled surfaces (Fig. 5*C*). The 12-Hz decrease in firing rate from FIX to PROBE task is modeled by the intercept parameter (for specific regression parameters for both tasks, see figure legend). Data from 2 additional neurons illustrate the opposite case, in which a neuron's firing rate is increased during PROBE task (Fig. 5*D*,*E*). The modeled surface in Fig. 5*F* shows a peaked response for both task blocks. In contrast, Fig. 5*G*,*H* shows a localized response of a neuron around the lower vertical meridian and neighboring positions. The resulting surface has a saddle-shaped receptive field spanning over the lower hemifield (Fig. 5*I*).

The effect of the loci of attention can be summarized for the population of 15 neurons (GØ, GSp) by computing a gain index solely using the intercept values $GI = (b_p - b_f)/(b_p + b_f)$, where b_f is the intercept value for the FIX receptive field (Tf_b in eqs. 2 and 3). The value b_p is the intercept for PROBE trials ($p_b + Tf_b$ in eqs. 2 and 3). Positive GI values describe cells that fired more to the stimulus during FIX trials, and negative values indicate a cell that fired more during PROBE trials. The even distribution of this index suggests that both enhancement and suppression is found under these conditions. The enhancement versus

suppression effects were independent of the order that the animal performed the 2 behavioral blocks.

GxSp Neurons

The remaining 15 of the 30 task-selective cells had an interaction between the task block and stimulus position. These cells changed their spatial selectivity dependent on the task and were examined quantitatively using the full categorical regression (eq. 4). This model permitted the linear and quadratic coefficients to depend on the task block as well as the intercept. The regression model fit 13 of the 15 cells significantly. Eight of these 13 significant cells were fit with quadratic parameters or a combination of quadratic and linear parameters in one or both blocks, and the remaining 5 cells yielded different linear receptive fields during both blocks.

Three examples of spatially complex modulation are illustrated in Figure 6. The neuron illustrated in Figure 6*A,B* responds weakly to all stimulus positions in the FIX task. When the animal performs the PROBE task, there is a clear preference for stimuli in the left visual field close to the midline. The corresponding modeled receptive fields intersect, with the FIX receptive field appearing rather flat and the PROBE receptive field showing a peaked response along the left horizontal meridian (Fig. 6*C*). Figure 6*D,E* illustrates a cell with a receptive field that shifts across the midline. In the FIX task, the receptive field is located in the left hemifield, whereas in the PROBE task, the receptive field shifts across the vertical meridian to the right visual field. This is indicated by a change in the sign of the horizontal linear coefficient (Fig. 6*F*). Finally, the last cell shown responds to stimuli in multiple distant positions but mostly in

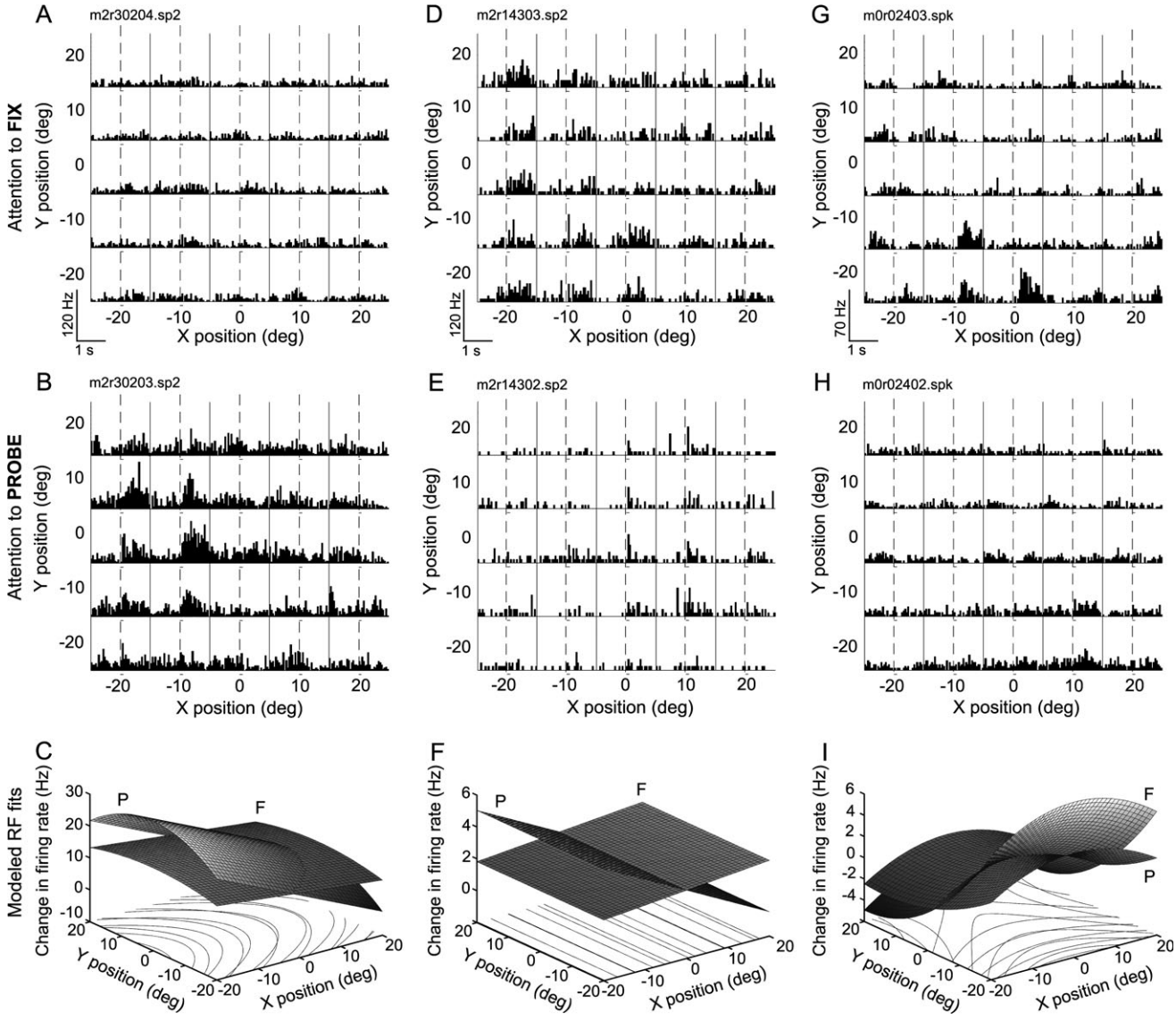

Figure 6. Peristimulus time histograms and quantitative fits for 3 representative G × Sp cells with interactions of the main effects. These cells had a change in spatial tuning that depended on task type. Conventions as in Figure 5. (*A–C*) Neuron that has a weak linear dependence during FIX trials (*A*). $A_{FIX} = -0.148x + 0.007y^2 + 3.04$. During PROBE trials (*B*), the baseline activity increases, and the neuron responds strongly to stimuli appearing in the left central visual field. $A_{PROBE} = -0.607x - 0.023y^2 + 8.61$. The tuning for stimuli appearing in the center of the visual field results in a response field that has a negative quadratic dependence along the *y* axis (*C*). (*D–F*) A cell that had a mirror reversal of tuning depending on attention. The cell is broadly tuned for stimuli in the left hemifield during FIX trials (*D*), $A_{FIX} = 0.023x + 2.29$, and becomes weakly tuned for stimuli toward the right during PROBE trials (*E*), $A_{PROBE} = -0.138x + 2.29$. In addition, attention to the stimulus during PROBE trials results in a suppression of this cell's baseline activity. (*G–I*) Neuron with saddle-shaped receptive fields in both tasks. $A_{FIX} = 0.264y - 0.0075x^2 + 0.0069y^2 + 0.57$; $A_{PROBE} = 0.093y - 0.0064x^2 + 0.0035y^2 + 0.57$.

the lower left quadrant and lower midline of the FIX condition (Fig. 6*G*) and shifts to a preference in the lower right quadrant during the PROBE task (Fig. 6*H*). This results in 2 intersecting saddle-shaped receptive fields (Fig. 6*I*).

Quantitative Receptive Field Structure

One goal of this study was to extract a more precise receptive field structure for 7a neurons by using a dense grid of mapping stimuli. The 5 × 5 grid of stimuli yielded the following types of receptive fields. Of the visually responsive neurons, 62% (47/76) were fit with at least one significant spatial parameter (a_x, a_y, a_{xx}, a_{yy}, a_{xy}) during either FIX or PROBE trials. Eleven of these 47 cells (23%) were only linearly modulated by the stimulus position. In these linear cases, the visual field representation of the response can be shown by plotting the horizontal (a_x) and vertical (a_y) terms. Another 77% (36/47) cells had a quadratic dependence in at least one dimension. In those cases, various parameters of spatial receptive fields can be extracted by the quadratic model such as the location, the shape, and the width of the receptive fields.

Visual Field Representation

To examine the representation of visual field with our detailed mapping data, the linear and quadratic regression coefficients were examined. For cells with linear coefficients, the hemifield with a maximal response could be evaluated by the sign of the coefficients. The mean vector was calculated for each animal from the a_x and a_y coefficients. A plot of these linear coefficients confirms that receptive fields are mostly confined to the lower contralateral visual quadrant in both monkeys (Fig. 7*A*).

For cells with quadratic components, the horizontal or vertical position that resulted in a maximum or minimum firing rate was computed for the data best modeled by a quadratic from the equation $(dA/dx)(X_c) = 0$ with a similar equation for Y_c (Fig. 7*B*). The receptive field centers in the horizontal (X_c) were normally distributed and symmetrically clustered around zero. The receptive field centers in the vertical (Y_c) were skewed to negative values suggesting a lower field bias in both task conditions. In mixed cases, for example a linear a_x and a quadratic a_{yy}, the quadratic term was used to locate the (Y_c) receptive field center. The horizontal component (a_x) has no center but rather extends beyond the edge of the receptive field testing. This was plotted as a point (Y_c) with 32° eccentricity for the horizontal (X_c) with the appropriate sign. The same procedure was used for quadratic (a_{xx}) and linear (a_y) combinations.

Receptive Field Shapes

To examine the receptive field shapes for the quadratic regression cases, the quadratic terms (a_{xx}, a_{yy}) were plotted for these neurons. In Figure 8*A–D*, the signs of the quadratic function for the receptive field center location (X_c, Y_c) are indicated. (The signs indicate whether the receptive field center is at a peak or a trough.) For both axes (compare Fig. 8*A*,*C* and 8*B*,*D*) and for both tasks (compare Fig. 8*A*,*B* and 8*C*,*D*), peaks and troughs can be found with similar frequency suggesting no bias for the receptive field center type. Furthermore, no trend was found toward local minima in the fovea, which would suggest foveal sparing.

Of the 8 cells fit with different signed quadratic terms in the horizontal and vertical dimensions, the saddle point was computed from (X_c, Y_c). These saddle points were scattered through all 4 quadrants, and there was insufficient data to examine receptive field properties for these cells.

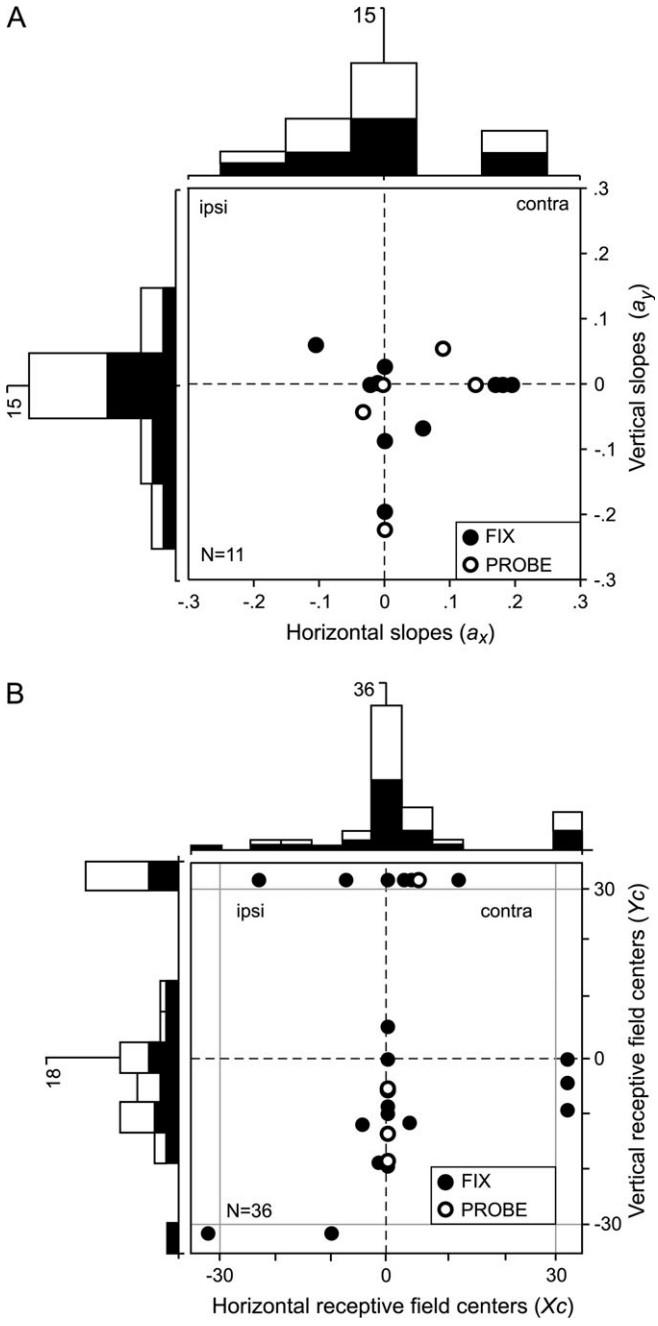

Figure 7. Visual field locations of receptive fields from linear and quadratic coefficients. All values are corrected for hemisphere and visual field for each animal (monkey S multiplied by −1). (*A*) Distribution of the linear terms (a_x, a_y) as derived from quantitative regression of firing rates. Horizontal and vertical terms (slopes) were plotted against each other. Distributions of these terms are plotted as histograms on the corresponding axes (filled bars, FIX trials; open bars, PROBE trials). (*B*) Horizontal and vertical coordinates reflecting receptive field centers derived from quadratic coefficients (X_c, Y_c). Filled circles depict centers during FIX trials and open circles depict centers during PROBE trials. Distributions of receptive field centers appear as histograms on the corresponding axes (same conventions as in *A*).

Receptive Field Spatial Bandwidth

The receptive field width was calculated from the amplitude of the quadratic regression coefficient. There was no difference

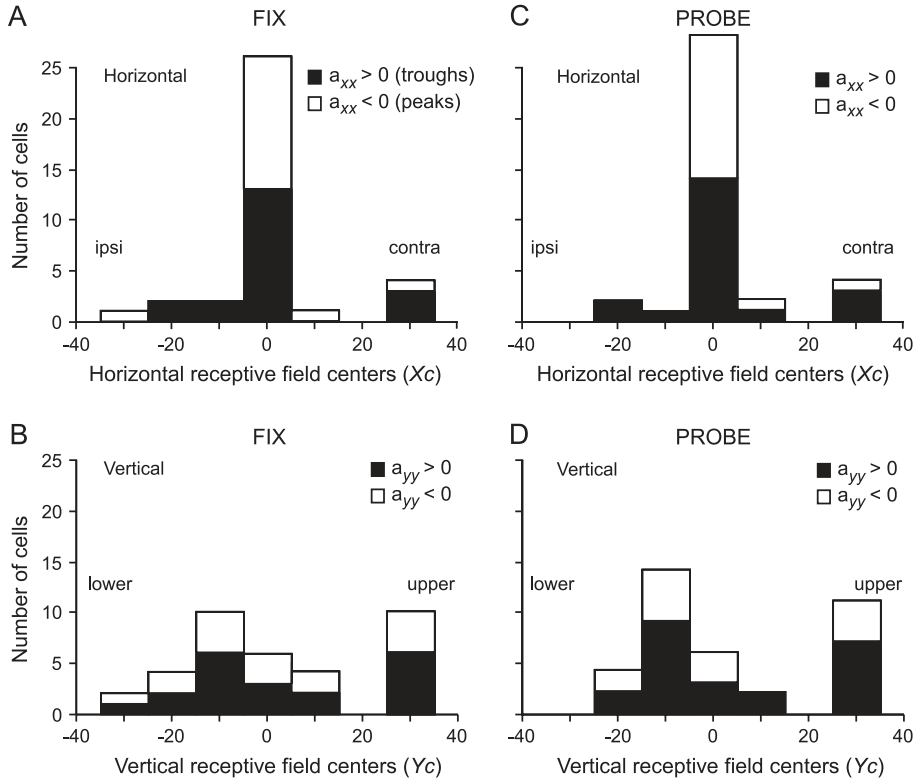

Figure 8. Distribution of signs for quadratic coefficients (a_{xx}, *A*, *C*; a_{yy}, *B*, *D*) of fit as a function of receptive field center during FIX trials (*A*, *B*) and during PROBE trials (*C*, *D*). Receptive field centers are corrected for hemisphere and visual field for each animal (monkey S multiplied by −1). Filled bars indicate cells with positive coefficients and reflect a center that is an RF minimum (trough). Open bars reflect negative coefficients of fit and centers that are RF maxima (peaks).

between the distributions of the half-height values for the 2 behavioral tasks (Fig. 9). The average bandwidth was 62° along the horizontal and 67° along the vertical. Furthermore, no correlation between bandwidth and receptive field center position (eccentricity) was found in either behavioral task.

Validation of the Unique Identity of a Neuron between FIX versus BLOCK Condition

Interspike interval return maps were computed for the FIX and PROBE conditions (Methods; Fig. 10). The interspike interval histograms demonstrate a traditional view of a neuron's temporal patterns. Peaks at ~10 ms are observed for both FIX and PROBE, followed by a roughly exponential decay (Fig. 10*A*,*D*). Interspike interval return maps were computed by plotting the *i*th interval versus the $i + 1$th interval (Fig. 10*B*,*D*). A clustering of short intervals followed by short interval can be observed by the density of the points close to the origin for both task conditions. Further, short intervals tend to follow long ones and vice versa as evidenced by the points near the ordinate and abscissa. Additional structure is revealed when these data are plotted on a logarithmic (base 10) scale. The example pair also illustrates that the structure is very similar for the FIX and PROBE runs (Fig. 10*C*,*F*).

Examination of the 106 pairs (FIX vs. PROBE) reveals that the interspike interval return maps, as shown in Figure 10*C*,*F*, have a range of unique structures. Four additional pairs of return maps illustrate some of the range of temporal patterns that can be observed (Fig. 11). Various bands and clusters in each of these plots indicate particular combinations of interspike intervals favored by a neuron. Each of the pairs is extremely similar, yet each neuron is quite different from the others.

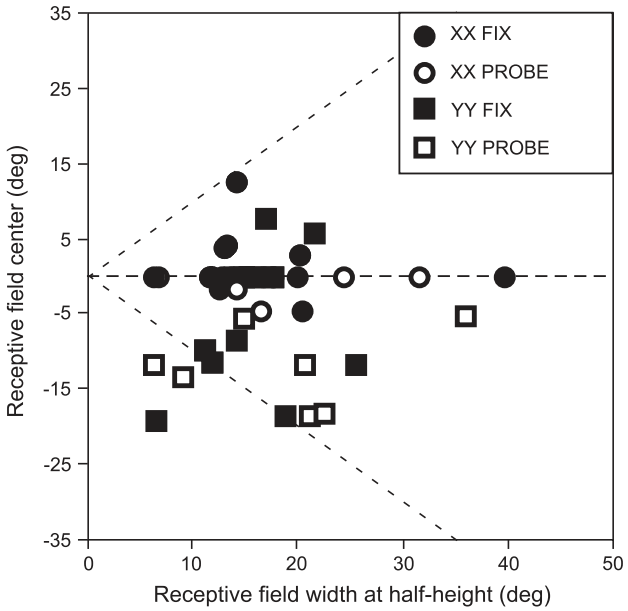

Figure 9. Receptive field width at half-height calculated from quadratic terms. Bandwidths are plotted for cells with negative quadratic fits as a function of the locations of their corresponding receptive field maxima (peaks) separately for the 2 axes (circles, horizontal; squares, vertical) and the 2 tasks (filled symbols, FIX task; open symbols, PROBE task). Dashed lines indicate unity lines if receptive field centers were proportional to receptive field width.

This observation was quantified by computing a 2-dimensional distribution of the density of points in the log-log return maps for every test of every neuron (see Methods). Each was normalized to a total volume under the surface of 1. The RMS

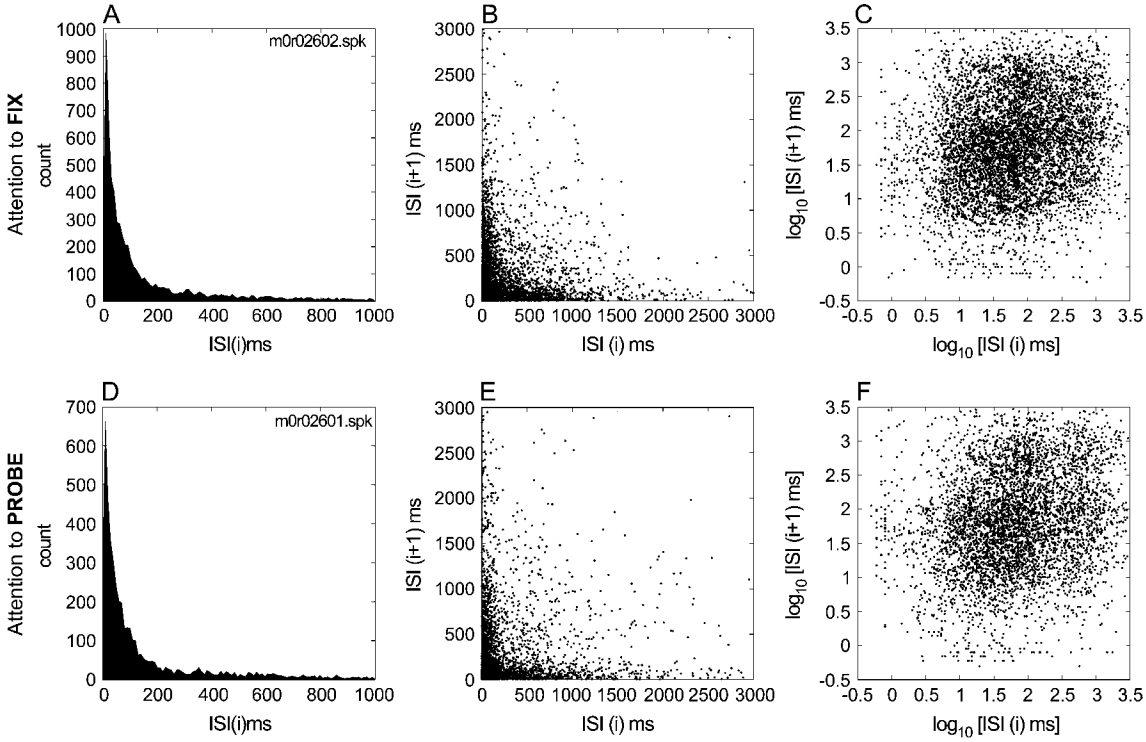

Figure 10. Temporal patterns of neural activity for a G × Sp neuron. (*A*, *D*) Interspike interval (ISI) histograms for both experimental conditions (FIX vs. PROBE). (*B*, *E*) Interspike interval return maps plotting the *i*th interval versus the $i + 1$th interval. (*C*, *F*) Interspike interval return maps on a logarithmic scale (base 10).

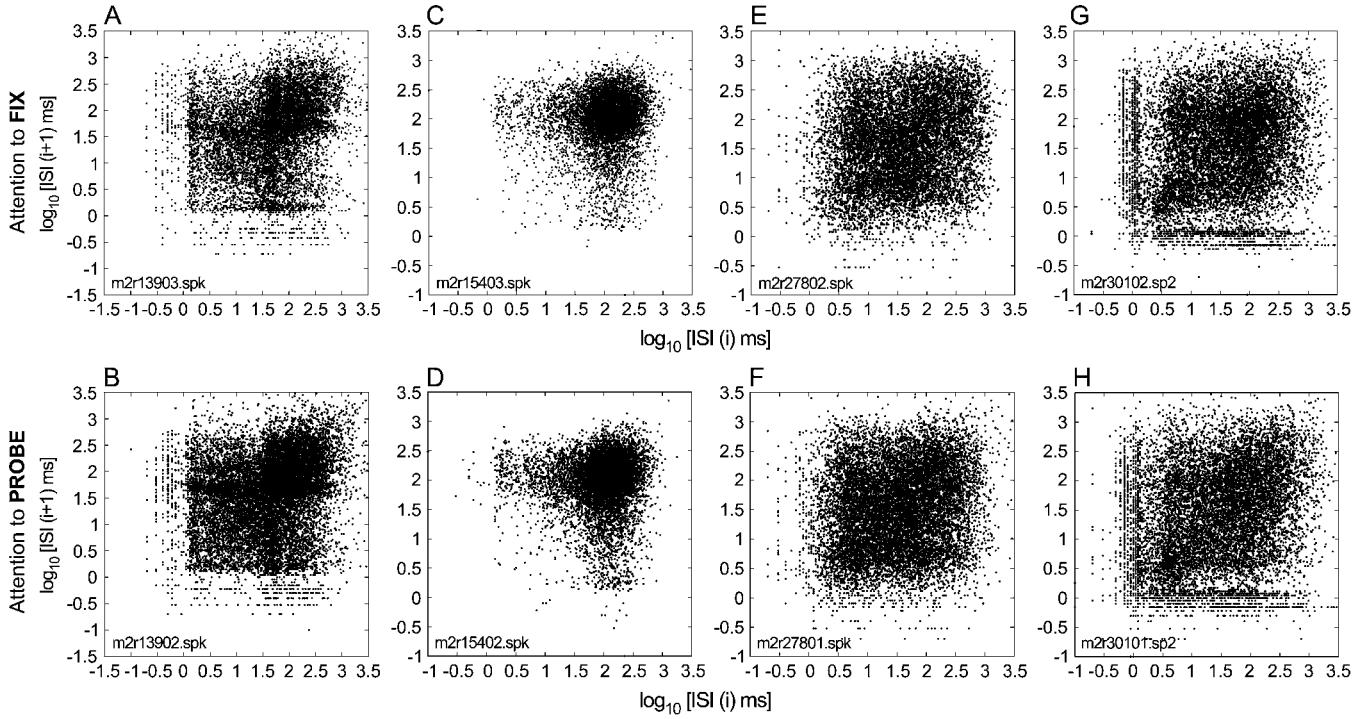

Figure 11. Samples of various temporal patterns. Interspike interval return maps for 4 neurons under each experimental condition (FIX vs. PROBE). (*A*, *B*) m2r13903/02.spk. (*C*, *D*) m2r15403/02.spk. (*E*, *F*) m2r27802/01.spk. (*G*, *H*) m2r30102/01.sp2.

of the difference between all possible pairs was then computed (Fig. 12). This set of all possible pairs contained "synthetic" pairings and the "actual" pairings. The resulting set of RMS values was split into 2 groups: those from actual FIX versus PROBE pairings and those synthetically generated by all the other pairings (Fig. 12*A*). A distribution of the RMS values for each group indicates that the distribution of RMS values was different for the actual group versus the synthetic group as

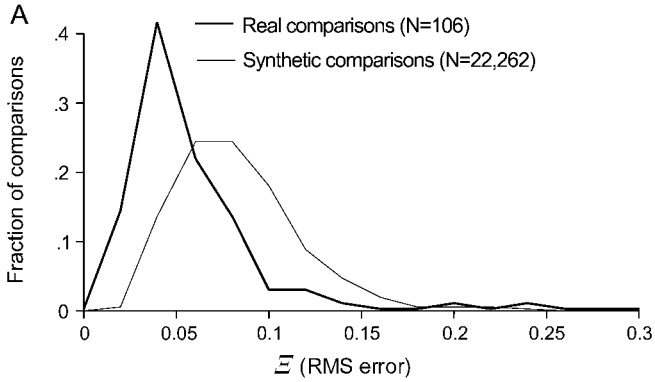

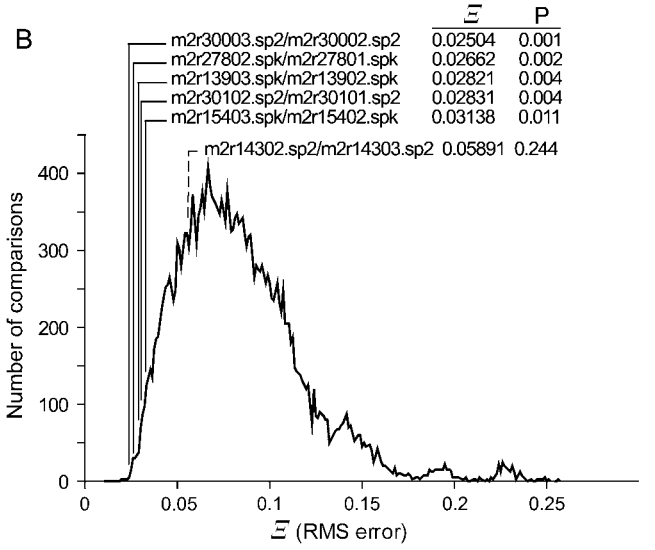

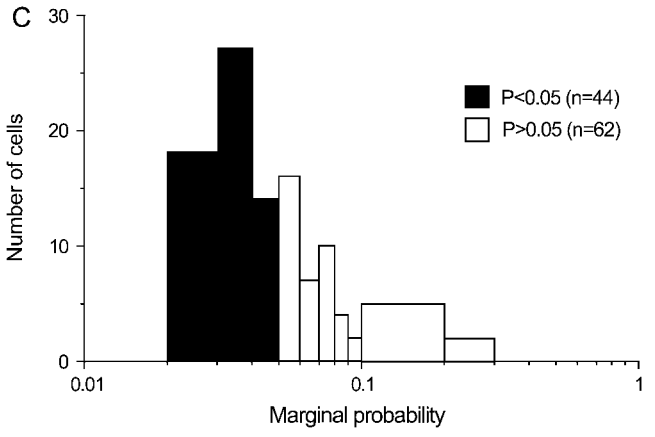

Figure 12. Statistical analysis of temporal patterns. (*A*) The root mean square (RMS) error of the difference, termed , computed for actual (PROBE vs. FIX) and synthetic (all possible) combinations of neurons and experiments. (*B*) Distribution of , for all paired comparisons at higher resolution. The location of 4 significant and 1 nonsignificant cell pair and their respective RMS errors and *P* values are indicated on the curve. (*C*) Plot of marginal probability (*P* values) for all actual comparisons.

confirmed by Kolmogorov–Smirnov goodness-of-fit test ($P < 0.001$). Figure 12*B* shows a fine-grained plot of Ξ for all combinations and the location of 4 significant sample cells and 1 nonsignificant cell.

Further, the marginal probability was computed for all the actual pairings by determining the fraction of measurements with RMS values less than a particular neuron. The distribution of these probabilities for the 106 cells (Fig. 12*C*) demonstrates that 44 of the cells had marginal probabilities less than 0.05. The remaining 62/106 neurons had a marginal probability greater than or equal to 0.05. (Such a neuron is noted in Fig. 12*B* by the dashed line.) Fifty-five of these 62 neurons could be explained by a substantial difference in the firing rate between the FIX and PROBE conditions. Visual inspection only revealed one pair that had characteristics indicating different interspike interval return maps and different temporal signatures, and 6 pairs were ambiguous. These results indicate that FIX and PROBE runs were likely being recorded from a single neuron with the same temporal pattern throughout the experimental session. None of these last 6 pairs were of the GSp category.

Discussion

Single units were recorded from area 7a, and the receptive fields were mapped while monkeys performed 2 tasks with differing attentional demands. Below, the properties of the receptive fields are summarized, followed by a discussion of the effect of the task on the monkeys' behavior and upon activity of single cells in area 7a.

Chaos Theory as a Means to Validate Recordings

With 25 experimental stimulus positions to test, these experiments required rather long periods of recordings (2–4 h). Typically, there is little question that the same neuron is held throughout a recording session, and one experimental condition can be repeated to mark the stability of the neuronal recording. In our study, it was rare that a neuron was held long enough to repeat the original experiment and the monkeys would perform sufficient trials. There is a valid concern that the change in tuning observed could be a result of a change in the isolation from one neuron to another. One means to support the continued isolation of a single unit is to compare the analog-sampled waveform; such data were not collected in this study and waveforms can change. Hence a different approach was used; a temporal signature or fingerprint was obtained using the interspike interval return map.

Quantitatively, it was not possible to distinguish the temporal patterns of activity between the 2 test blocks making it likely that the same neuron was held throughout the experiment. This approach may be useful in other situations where the long-term recording and the behavioral conditions may preclude repeating certain experiments. Future work with the RMS error measure (Ξ) should incorporate the number of spikes. Although it is possible that changes in the temporal signatures may occur as a result of experimental manipulations, perhaps indicating changes in the underlying connectivity, this does not appear to be the case in the attentional paradigm used here. Among the 30 neurons with a change in receptive field shape (GØ, GSp, or G × Sp class), none showed a change in the temporal pattern as assessed here.

Quantitative Receptive Field Properties

In order to quantitatively describe receptive fields, retinotopic positions were sampled at high resolution. A quadratic regression modeled the firing rate of each neuron taking into account intertrial variance. A stepwise procedure selected the number of variables incorporated into the model (Read and Siegel 1997). This approach is an advance over earlier studies

that used coarser sampling to conclude that area 7a neurons have large, nonuniform bilateral receptive fields (Sakata et al. 1980; Motter and Mountcastle 1981; Mountcastle et al. 1981) or which did not quantify the receptive field properties (Andersen, Asanuma, et al. 1990). The current study mapped neural responses over the same area as a previous study (Read and Siegel 1997) but used a smaller probe stimulus (5°) appearing at 25 instead of 9 visual field positions. This resulted in a finer grained map of receptive fields.

In general, and in agreement with prior studies, area 7a receptive fields were usually large and bilateral (Motter and Mountcastle 1981; Andersen et al. 1985; Andersen, Asanuma, et al. 1990). Approximately one-fourth were spatially tuned in a linear fashion, with a bias for stimuli appearing in the contralateral hemifield, confirming other studies (Andersen, Asanuma, et al. 1990; Ben Hamed et al. 2001; Battaglia-Mayer et al. 2005; Heider et al. 2005). Other cells were well modeled with quadratic response fields indicating either a "peaked" response profile for those cells with receptive field maximum or a U-shaped response profile for those with a receptive field "trough."

The receptive field width measurements of quadratic (i.e., parabolic) response fields at half-height (termed bandwidth) indicate that area 7a cells have receptive field widths that average around 60° at half-peak activity and are largely centered over the fovea. This width measurement compares well with previous reports (Andersen, Asanuma, et al. 1990), in which the average receptive field width using a Gaussian tuning fit was 44° at a fall off point of 1/e below peak activity (see their Fig. 26). Extrapolation of the half-height activity for this fit (63°) was found to be in agreement with the present results.

Interestingly, parabolic receptive fields were usually found only along one dimension. Prior studies in areas 7a and LIP, the inferior parietal lobule, have reported circular receptive fields with little consistency in breadth and in fact have emphasized their size variability (Andersen, Asanuma, et al. 1990; Blatt et al. 1990). The more detailed mapping in combination with the quantitative regression of the current study permits a better estimate of the receptive field shape. These current data suggest that area 7a receptive fields sample elongated regions of the visual field that are fairly consistent in breadth, irrespective of the meridian along which selectivity lies. Studies in other, mostly earlier visual areas (e.g., areas V1 to V4, but also LIP) demonstrate a roughly linear relationship between eccentricity of receptive field centers and receptive field size (Van Essen and Maunsell 1980; Gattass et al. 1981, 1988; Dow et al. 1985; Ben Hamed et al. 2001).

The detailed study of receptive field structure permits yet another reexamination of "foveal sparing" (Motter and Mountcastle 1981; Andersen, Asanuma, et al. 1990), that is, reduced activity of area 7a neurons to stimuli presented at the foveal region. Later studies have described a subpopulation of cells with a "peaked" receptive field configuration, that is, in which a zone of maximum evoked response occurs for foveal stimuli (Andersen, Bracewell, et al. 1990b; Andersen 1995; Read and Siegel 1997). Foveal sparing has been attributed to an effect of guided attention at the foveal region (Constantinidis and Steinmetz 1996). Such receptive fields would show a minimum response for stimuli in the center. Among our population of modeled receptive fields, we did not find a plethora of receptive fields of this shape. Thus, the current data provide no evidence for foveal sparing under either attentional condition. However, one has also to consider the relatively small number of cells and the reduced visual field sampling compared with previous studies, that is, 40° × 40° in the current study versus 60° × 200° in the study by Motter et al. (1981).

Reaction Time Dependence on Task

Spatial attention was modulated by 2 tasks in which the monkeys had to fixate the central fixation point throughout the entire trial. In the FIX task, the monkeys had to respond to the dimming of the red 0.5° fixation point, whereas in the PROBE task, the monkeys had to respond to a dimming 5° white square. FIX and PROBE trials were delivered in separate blocks. Retinal stimulation in the 2 tasks was identical with successful performance based upon the 2 attentional rules. Analysis of reaction times confirmed that the behavior differed between the 2 tasks. When the animal was responding to the dimming of the fixation point (FIX task), the reaction times did not vary with probe location. In the blocks where the animal responded to the dimming of the probe (PROBE task), the reaction times varied with probe location. In most of these cases, eccentric targets yielded longer reaction times. This suggests that the monkey adjusted his strategy according to the demands of the task. Moreover, the shifts in reaction time pattern were similar for both monkeys, supporting the conclusion that the intended systematic behavioral rule was used. Similar effects of eccentricity on reaction times have been found in humans (Carrasco et al. 1995; Carrasco and Yeshurun 1998).

An important issue to consider is whether the reaction time difference between the 2 tasks was due to difficulty. Error rates were generally low and comparable between the 2 types of task (~90% correct). Thus, it is unlikely that differences in task difficulty are a sufficient explanation for the asymmetry in neural responses described below.

A third issue is the time course of attention during the entire task. The probe dimmed over the interval 3500–5500 ms following the start of the trial (i.e., 1500–3500 ms after probe onset). It is reasonable to suggest that the monkeys' attention shifted just after the time of probe onset. Similar reasoning was suggested for changes in neural responses evaluated prior to eye movements (Bushnell et al. 1981). To conclude, the difference of reaction time profiles under the 2 task conditions supports the assumption that the monkeys used 2 different spatial attentional strategies.

Neural Activity Dependence on Task

Baseline Firing Rate

For the purpose of this study, baseline firing rate was defined as the activity of a neuron prior to probe stimulus onset while the animal was engaged in the behavioral task (i.e., active fixation). A substantial proportion of area 7a neurons (two-thirds) showed a dependency of baseline firing rate on the behavioral task. An explanation for differences in baseline activity might be due to the order in which blocks were delivered. Effects of novelty and repetitive stimulation have been reported in area 7a (Steinmetz et al. 1994). However, the direction of the effect did not depend on which block was first presented. Hence, it is likely that the changes in the baseline firing rate are correlated with the task. Possible behavioral correlates are the effect of expectation, as seen in visual areas as early as V3A (Nakamura and Colby 2000), or the type of task. It is worth remarking that both enhancement and suppression of the baseline firing rate were observed with

either task. Whether the range of effects could be mapped to a cortical functional architecture in 7a is an open question to be explored using optical mapping techniques.

Receptive Field Modulation

The receptive fields of area 7a neurons were analyzed with a statistically rigorous implementation of classical mapping methods using the well-understood general linear model. The behavioral task was correlated with changes in the visual response in almost 30% of the neurons. Two types of modulation were observed with equal frequency. The first type of modulation involved an additive scaling of spatial tuning by attention similar to that described in area 7a (Bushnell et al. 1981; Motter and Mountcastle 1981; Constantinidis and Steinmetz 1996). Both enhancement and suppression were found unlike earlier studies that emphasized one or the other. Other studies found a "push–pull" form of modulation in areas 7a (Bender and Youakim 2001) and nearby parietal area LIP (Ben Hamed et al. 2002), in which some cells were facilitated and others suppressed during different attentive modes of behavior; the current results are most similar to these. Thus, changes in the attentional state can have both excitatory and inhibitory effects on the firing rate of neurons without altering the receptive field shape.

The second type of modulation was a multiplicative interaction of positional and attentional variables. This resulted in shifts of the receptive field center (i.e., maxima or minima) across the visual field. To our knowledge, such cells have not yet been described in area 7a. Attentional shifts in receptive field centers have been described in visual area V4 (Connor et al. 1996, 1997), MT (Womelsdorf et al. 2006), and LIP (Ben Hamed et al. 2002). There are also receptive field shifts prior to eye movements in V4 (Tolias et al. 2001); for area 7a to be involved in these responses would require activity propagating back through a series of projections to V4. A similar result found for area 7a is the alteration of neuronal responses while a monkey "mentally" follows a route in a maze while fixating (Crowe et al. 2004). This study shows path-tuning functions during maze solution that were not aligned to visual receptive fields mapped outside the context of maze solution and suggests that the path tuning of area 7a neurons reflects their participation in a goal-driven spatial analysis of visual maze stimuli.

There may be similar mechanisms at play in the current study, where about 20% of visually responsive cells showed an effect of task. Receptive field shifts in the current study suggest changes up to 20°. What is particularly intriguing is that cells can switch from contralateral to ipsilateral receptive fields. This is congruent with optically reported effects of attention (Raffi and Siegel 2005). A recent study found that spatial attention can affect receptive field shape of area MT neurons even from the opposite hemifield (Womelsdorf et al. 2006).

One other possibility for the change in tuning observed across blocks is a spontaneous change in the receptive field properties that is independent of task. Due to the duration of the recording session, it was not possible to repeat the initial block a second time, and identical blocks were rarely run in succession. To properly test the stability and stationarity of the properties of a neuron, experiments are needed wherein a single cell is recorded under a single set of conditions for many hours to determine if there are systematic shifts in its response properties. To our knowledge, no such studies have been performed in the inferior parietal lobule, although computational techniques for testing stationarity of neuronal response are being derived (Grun et al. 2002).

Ramification for Optical Imaging Studies of Retinotopy in Area 7a

The receptive field shapes observed electrophysiologically were a mix of linear and quadratic models. In the optical imaging study of area 7a retinotopy (Heider et al. 2005), predominantly linear retinotopic activation was selected as the best model using the Akaike Information Criterion (Akaike 1974). The inability to observe quadratic retinotopic structure with optical imaging in this area may arise from biological or numerical constraints. Numerically, the optical data have a lower signal-to-noise ratio than the electrophysiological data which, in principle, could make it more difficult to resolve quadratic receptive fields. However, in the same optical study, peaked quadratic retinotopic activation was observed in other cortical regions (i.e., early visual cortex V1 and V2), indicating that the signal-to-noise ratio was not the issue.

Biologically, there are differences in the quantities measured electrophysiologically and optically. The optical measurements are from the upper layers (e.g., layers I, II/III) of the cortex and predominantly indicate metabolism from subthreshold activity of small-diameter pre- and postsynaptic fibers (Logothetis et al. 2001; Vanzetta et al. 2005). The electrical measurements are taken from all layers and generally indicate somatic spiking. Thus, it may be that small fiber elements are modulated linearly, and these receptive fields are modulated into quadratic shape via spatial–temporal interaction in the dendritic tree and soma. Alternatively, the linear receptive fields are limited to the upper layers. To our knowledge, no data are available to distinguish between these possibilities.

Although there were differences in the quantitative receptive field shapes reported optically and electrophysiologically, one feature is found with both types of measurements. In both studies, the center of the receptive fields can shift. In the optical studies, the same cortical region was studied across days, and the retinotopic activation derived from these measurements was variable (Heider et al. 2005). In the electrophysiological studies reported here, the receptive field center can shift. We speculate that the same mechanism may be responsible for the receptive field shift in both studies, the mechanism being an ongoing allocation of resources to fit the attentional needs at the moment (Raffi and Siegel 2005). Various neural circuits could be devised to drive such a mechanism; these are beyond the scope of this report.

Support for the Complexity of Receptive Fields

Allman et al. (1985) stressed that the receptive field structure in various visual areas does not always align with classical concepts. Much of that review indicates how receptive field could be influenced by visual input spatially distant from the receptive field center. Their work allowed for extraretinal modulation, although electrophysiological examples at that time indicated a gain-like effect. Certainly, spatial attention is well known to have an amplitude-modifying influence on receptive fields in parietal (Robinson et al. 1980; Bushnell et al. 1981; Mountcastle et al. 1981; Motter 1998; Tootell et al. 1998; Constantinidis and Steinmetz 2001; Ben Hamed et al. 2002) and other areas such as V1 (Gilbert 1993). Previous

studies of area 7a also suggest that neurons are modulated by a variety of extraretinal factors, for example, orbital eye position, reaching movements, and motivational factors, among others (Sakata et al. 1980; Hyvarinen 1981; Mountcastle et al. 1981; Andersen, Bracewell, et al. 1990; MacKay 1992; Constantinidis and Steinmetz 1996, 2001). The current work demonstrates similar attentional gain-like extraretinal effects of attention in area 7a.

Importantly, a new modulation has been discovered whereby the receptive field can be shifted in retinal coordinates as a function of the task state. A shifting of the receptive field location by attention leads to a novel set of questions. How can the projective cortices (e.g., prefrontal cortex) read out the receptive field signal from area 7a if the receptive field center changes? A mainstay of the contemporary concept of cortical organization has been the classic idea of "specific nerve energy" (Müller 1833), also termed the "loop-line" (James 1890), or "labeled-line hypothesis" (Helmholtz 1867). It is the proposal that the axon leading from a neuron carries a signal best responding to a particular sensory event (cf. Llinás 2001). Under this hypothesis, these events, such as retinotopic location of a visual stimulus, are expected to be constant across time, so that a signal from an axon can reliably be interpreted. From these temporally constant signals, cortex can be organized into maps for many species. How can the recipient cortex interpret a sequence of action potentials from a neuron whose spatial tuning changes over time, from a cell whose label can change?

In the present study, the animal's attentional locus can change the receptive field center assessed electrophysiologically. Presumably, these receptive fields are organized across the cortical surface in a map similar to that described from optical measurements (Heider et al. 2005). Shifts in the receptive field centers ought to modify the topography of retinotopy. Indeed, optical measurements under a somewhat different attentional task suggest that patches of cortex are modulated by attentional shifts (Raffi and Siegel 2005). Such an attentional effect on retinotopy might also help to explain a recent study demonstrating that attentive tracking of a moving stimulus can shift the perceived stimulus location (Shim and Cavanagh 2005).

One means whereby the projective cortices of area 7a, such as prefrontal cortex, can properly interpret such complex and varying multidimensional signals is by a constant interchange of neuronal activity. This would permit 2 areas both to vary and to work as a unit toward solving the behavioral task of the moment. Possible implementations might be a shifter circuit (Anderson and Van Essen 1987) that operated bidirectionally or by reentry (Edelman 1989). Although this is highly speculative, the constant interplay of signals between pairs of areas, and within each area, would enable a rich repertoire of heterogeneous parameters within area 7a, for example, optic flow (Siegel and Read 1997a; Phinney and Siegel 2000), gain field (Andersen, Bracewell, et al. 1990; Read and Siegel 1997; Siegel et al. 2003), attention (Sakata et al. 1980; Steinmetz and Constantinidis 1995; Raffi and Siegel 2005), and stimulus disparity (Phinney and Siegel 1999) to be represented in a relatively small parcel of cortex. As well, the constant interactions would permit the selection of the right set of parameters from the combinatorial complex space leading to a simplified and transient selectivity. This would permit neurons tuned to multiple stimulus and behavioral dimensions to participate in a range of tasks. Presumably, the intrinsic network connectivity within area 7a and its connections that cull information from multiple stimulus and internal-state dimensions are involved in constructing a dynamic sensorimotor representation of extrapersonal space without the use of static labeled lines.

Notes

The excellent technical assistance of Daniela Dimichino and Babatunde Orogbemi is acknowledged. Supported by NIH/EY09223, NIH/NCRR12873, and NIH/DA11687; The Whitehall Foundation; and National Science Foundation Grant NPACI RUT223. Computational resources of the Center for Computational Neuroscience, Rutgers University, Newark, are acknowledged. *Conflict of Interest*: None declared.

Address correspondence to email: axon@cortex.rutgers.edu.

References

Akaike H. 1974. A new look at the statistical model identification. IEEE Trans Automatic Control. 19:716–723.

Allman J, Miezin F, McGuinness E. 1985. Stimulus specific responses from beyond the classical receptive field: neurophysiological mechanisms for local-global comparison in visual neurons. Annu Rev Neurosci. 8:407–430.

Andersen RA. 1995. Encoding of intention and spatial location in the posterior parietal cortex. Cereb Cortex. 5:457–469.

Andersen RA, Asanuma C, Essick G, Siegel RM. 1990. Corticocortical connections of anatomically and physiologically defined subdivisions within the inferior parietal lobule. J Comp Neurol. 296:65–113.

Andersen RA, Bracewell RM, Barash S, Gnadt JW, Fogassi L. 1990. Eye position effects on visual, memory, and saccade-related activity in areas LIP and 7a of macaque. J Neurosci. 10:1176–1196.

Andersen RA, Essick GK, Siegel RM. 1985. Encoding of spatial location by posterior parietal neurons. Science. 230:456–458.

Anderson CH, Van Essen DC. 1987. Shifter circuits: a computational strategy for dynamic aspects of visual processing. Proc Natl Acad Sci USA. 84:6297–6301.

Anderson KC, Siegel RM. 1999. Optic flow selectivity in the anterior superior temporal polysensory area, STPa, of the behaving monkey. J Neurosci. 19:2681–2692.

Bálint R. 1909. Seelenlähmung des "Schauens", optische Ataxie und räumliche Störung der Aufmerksamkeit. Monatsschr Psychiatr Neurol. 25:51–81.

Battaglia-Mayer A, Mascaro M, Brunamonti E, Caminiti R. 2005. The over-representation of contralateral space in parietal cortex: a positive image of directional motor components of neglect? Cereb Cortex. 15:514–525.

Ben Hamed S, Duhamel JR, Bremmer F, Graf W. 2001. Representation of the visual field in the lateral intraparietal area of macaque monkeys: a quantitative receptive field analysis. Exp Brain Res. 140:127–144.

Ben Hamed S, Duhamel J-R, Bremmer F, Graf W. 2002. Visual receptive field modulation in the lateral intraparietal area during attentive fixation and free gaze. Cereb Cortex. 12:234–245.

Bender DB, Youakim M. 2001. Effect of attentive fixation in macaque thalamus and cortex. J Neurophysiol. 85:219–234.

Bisiach E, Perani D, Vallar G, Berti A. 1986. Unilateral neglect: personal and extra-personal. Neuropsychologia. 24:759–767.

Blatt GJ, Andersen RA, Stoner GR. 1990. Visual receptive field organization and cortico-cortical connections of the lateral intraparietal area (area LIP) in the macaque. J Comp Neurol. 299:421–445.

Bushnell MC, Goldberg ME, Robinson DL. 1981. Behavioral enhancement of visual responses in monkey cerebral cortex. I. Modulation in posterior parietal cortex related to selective visual attention. J Neurophysiol. 46:755–772.

Carrasco M, Evert DL, Chang I, Katz SM. 1995. The eccentricity effect: target eccentricity affects performance on conjunction searches. Perception Psychophys. 57:1241–1261.

Carrasco M, Yeshurun Y. 1998. The contribution of covert attention to the set-size and eccentricity effects in visual search. J Exp Psychol Hum Percept Perform. 24:673–692.

Cavada C, Goldman-Rakic PS. 1989. Posterior parietal cortex in rhesus monkey: I. Parcellation of areas based on distinctive limbic and sensory corticocortical connections. J Comp Neurol 287:393–421.

Connor CE, Gallant JL, Preddie DC, Van Essen DC. 1996. Responses in area V4 depend on the spatial relationship between stimulus and attention. J Neurophysiol. 75:1306–1308.
Connor CE, Preddie DC, Gallant JL, Van Essen DC. 1997. Spatial attention effects in macaque area V4. J Neurosci 17:3201–3214.
Constantinidis C, Steinmetz MA. 1996. Neuronal activity in posterior parietal area 7a during the delay periods of a spatial memory task. J Neurophysiol. 76:1352–1355.
Constantinidis C, Steinmetz MA. 2001 Neuronal responses in area 7a to multiple-stimulus displays: I. Neurons encode the location of the salient stimulus. Cereb Cortex. 11:581–591.
Critchley M. 1978. Brain mechanisms for directed attention. J R Soc Med. 71:233.
Crowe DA, Chafee MV, Averbeck BB, Georgopoulos AP. 2004. Neural activity in primate parietal area 7a related to spatial analysis of visual mazes. Cereb Cortex. 14:23–34.
Desimone R, Duncan J. 1996. Neural mechanisms of selective visual attention. Annu Rev Neurosci. 18:193–222.
Dow BM, Vautin RG, Bauer R. 1985. The mapping of visual space onto foveal striate cortex in the macaque monkey. J Neurosci. 5:890–902.
Edelman GM. 1989. The remembered present: a biological theory of consciousness. New York: Basics Books.
Gaffan D, Hornak J. 1997. Visual neglect in the monkey. Representation and disconnection. Brain. 120:1647–1657.
Gattass R, Gross CG, Sandell JH. 1981. Visual topography of V2 in the macaque. J Comp Neurol 201:519–539.
Gattass R, Sousa APB, Gross CG. 1988. Visuotopic organization and extent of V3 and V4 of the macaque. J Neurosci. 8:1831–1845.
Gilbert CD. 1993. Circuitry, architecture, and functional dynamics of visual cortex. Cereb Cortex. 3:373–386.
Gnadt JW, Andersen RA. 1988. Memory related motor planning activity in posterior parietal cortex of macaque. Exp Brain Res. 70:216–220.
Goldberg ME, Bruce CJ. 1985. Cerebral cortical activity associated with the orientation of visual attention in the rhesus monkey. Vision Res. 25:471–481.
Goldberg ME, Wurtz RH. 1972. Activity of superior colliculus in behaving monkey. II. Effect of attention on neuronal responses. J Neurophysiol. 35:560–574.
Grun S, Diesmann M, Aertsen A. 2002. Unitary events in multiple single-neuron spiking activity: II. Nonstationary data. Neural Comput. 14:81–119.
Heider B, Jando G, Siegel RM. 2005. Functional architecture of retinotopy in visual association cortex of behaving monkey. Cereb Cortex. 15:460–478.
Helmholtz Hv. 1867. Handbuch der physiologischen Optik. Leibzig (Germany): Voss.
Hyvarinen J. 1981. Regional distribution of functions in parietal association area 7 of the monkey. Brain Res. 206:287–303.
James W. 1890. The principles of psychology. New York: Henry Holt.
Karnath HO, Fruhmann Berger M, Kuker W, Rorden C. 2004. The anatomy of spatial neglect based on voxelwise statistical analysis: a study of 140 patients. Cereb Cortex. 14:1164–1172.
Kastner S, Ungerleider LG. 2000. Mechanisms of visual attention in the human cortex. Annu Rev Neurosci 23:315–341.
Lewis JW, Van Essen DC. 2000a. Corticocortical connections of visual, sensorimotor, and multimodal processing areas in the parietal lobe of the macaque monkey. J Comp Neurol. 428:112–137.
Lewis JW, Van Essen DC. 2000b. Mapping of architectonic subdivisions in the macaque monkey, with emphasis on parieto-occipital cortex. J Comp Neurol. 428:79–111.
Llinás RR. 2001. I of the vortex: from neurons to self. Cambridge (MA): MIT Press.
Logothetis NK, Pauls J, Augath M, Trinath T, Oeltermann A. 2001. Neurophysiological investigation of the basis of the fMRI signal. Nature. 412:150–157.
Luck SJ, Chelazzi L, Hillyard SA, Desimone R. 1997. Neural mechanisms of spatial selective attention in areas V1, V2, and V4 of macaque visual cortex. J Neurophysiol. 77:24–42.
Lynch JC, Mountcastle VB, Talbot WH, Yin TC. 1977. Parietal lobe mechanisms for directed visual attention. J Neurophysiol. 40:362–389.
MacKay WA. 1992. Properties of reach-related neuronal activity in cortical area 7A. J Neurophysiol. 67:1335–1345.
Marshall JW, Baker HF, Ridley RM. 2002. Contralesional neglect in monkeys with small unilateral parietal cortical ablations. Behav Brain Res. 136:257–265.
Maunsell JH. 1995. The brain's visual world: representation of visual targets in cerebral cortex. Science. 270:764–769.
McAdams CJ, Maunsell JH. 1999. Effects of attention on the reliability of individual neurons in monkey visual cortex. Neuron. 23: 765–773.
Mesulam MM. 1999. Spatial attention and neglect: parietal, frontal and cingulate contributions to the mental representation and attentional targeting of salient extrapersonal events. Philos Trans R Soc Lond Ser B Biol Sci. 354:1325–1346.
Michel F, Henaff MA. 2004. Seeing without the occipito-parietal cortex: simultagnosia as a shrinkage of the attentional visual field. Behav Neurol. 15:3–13.
Moran J, Desimone R. 1985. Selective attention gates visual processing in the extrastriate cortex. Science. 229:782–784.
Motter BC. 1998. Inside and outside the focus of attention. Neuron. 21:951–953.
Motter BC, Mountcastle VB. 1981. The functional properties of the light-sensitive neurons of the posterior parietal cortex studied in waking monkeys: foveal sparing and opponent vector organization. J Neurosci. 1:3–26.
Mountcastle VB, Andersen RA, Motter BC. 1981. The influence of attentive fixation upon the excitability of the light-sensitive neurons of the posterior parietal cortex. J Neurosci. 1:1218–1225.
Mountcastle VB, Motter BC, Steinmetz MA, Sestokas AK. 1987. Common and differential effects of attentive fixation on the excitability of parietal and prestriate (V4) cortical visual neurons in the macaque monkey. J Neurosci. 7:2239–2255.
Müller JP. 1833. Handbuch der Physiologie des Menschen für Vorlesungen. Coblenz (Germany): Verlag von J. Hölscher.
Nakamura K, Colby CL. 2000. Visual, saccade-related, and cognitive activation of single neurons in monkey extrastriate area V3A. J Neurophysiol. 84:677–692.
Phinney RE, Siegel RM. 1999. Stored representations of three-dimensional objects in the absence of two-dimensional cues. Perception. 28:725–737.
Phinney RE, Siegel RM. 2000. Speed selectivity for optic flow in area 7a of the behaving macaque. Cereb Cortex. 10:413–421.
Quraishi S, Siegel RM. 1997a. Attentional modulation of parietal area 7a neurons in the awake behaving monkey. Investig Ophthalmol Vis Sci. 38:S625.
Quraishi S, Siegel RM. 1997b. Early and late effects of attention on receptive field properties in parietal area 7a of the behaving monkey. Soc Abstr Neurosci. 23:1546.
Raffi M, Siegel RM. 2005. Functional architecture of spatial attention in the parietal cortex of the behaving monkey. J Neurosci. 25:5171–5186.
Ratzlaff EH, Siegel RM. 1990. A workstation interface for measuring interspike intervals. J Neurosci Methods. 35:195–201.
Read HL, Siegel RM. 1996. The origins of aperiodicities in sensory neuron entrainment. Neuroscience. 75:301–314.
Read HL, Siegel RM. 1997. Modulation of responses to optic flow in area 7a by retinotopic and oculomotor cues in monkey. Cereb Cortex. 7:647–661.
Robinson DL, Baizer JS, Dow BM. 1980. Behavioral enhancement of visual responses of prestriate neurons of the rhesus monkey. Investig Ophthalmol Vis Sci. 19:1120–1123.
Rozzi S, Calzavara R, Belmalih A, Borra E, Gregoriou GG, Matelli M, Luppino G. 2006. Cortical connections of the inferior parietal cortical convexity of the macaque monkey. Cereb Cortex. 16:1389–1417.
Sakata H, Shibutani H, Kawano K. 1980. Spatial properties of visual fixation neurons in posterior parietal association cortex of the monkey. J Neurophysiol. 43:1654–1672.
Shim WM, Cavanagh P. 2005. Attentive tracking shifts the perceived location of a nearby flash. Vision Res. 45:3253–3261.

Siegel RM. 1990. Non-linear dynamical system theory and primary visual cortical processing. Physica D. 42:385–395.
Siegel RM, Raffi M, Phinney RE, Turner JA, Jando G. 2003. Functional architecture of eye position gain fields in visual association cortex of behaving monkey. J Neurophysiol. 90:1279–1294.
Siegel RM, Read HL. 1993a. Models of the temporal dynamics of visual processing. J Stat Phys. 70:297–308.
Siegel RM, Read HL. 1993b. Temporal processing in the visual brain. Ann N Y Acad Sci. 682:171–178.
Siegel RM, Read HL. 1997a. Analysis of optic flow in the monkey parietal area 7a. Cereb Cortex. 7:327–346.
Siegel RM, Read HL. 1997b. Construction and representation of visual space in the inferior parietal lobule. In: Rockland KS, Kaas JH, Peters A, editors. Extrastriate cortex in primates. New York: Plenum Press. p. 499–525.
Siegel RM, Read HL. 2001. Deterministic dynamics emerging from a cortical functional architecture. Neural Netw. 14:697–713.
Steinmetz MA, Connor CE, Constantinidis C, McLaughlin JR. 1994. Covert attention suppresses neuronal responses in area 7a of the posterior parietal cortex. J Neurophysiol. 72:1020–1023.
Steinmetz MA, Constantinidis C. 1995. Neurophysiological evidence for a role of posterior parietal cortex in redirecting visual attention. Cereb Cortex. 5:448–456.
Takens F. 1981. Detecting strange attractors in turbulence. In: Rand D, Young LS, editors. Dynamical systems and turbulence. Lecture notes in Mathematics. Berlin: Springer-Verlag. p. 366–381.
Tolias AS, Moore T, Smirnakis SM, Tehovnik EJ, Siapas AG, Schiller PH. 2001. Eye movements modulate visual receptive fields of V4 neurons. Neuron. 29:757–767.
Tootell RB, Hadjikhani N, Hall EK, Marrett S, Vanduffel W, Vaughan JT, Dale AM. 1998. The retinotopy of visual spatial attention. Neuron. 21:1409–1422.
Treue S, Martinez Trujillo JC. 1999. Feature-based attention influences motion processing gain in macaque visual cortex. Nature. 399:575–579.
Van Essen DC, Maunsell JH. 1980. Two-dimensional maps of the cerebral cortex. J Comp Neurol. 191:255–281.
Vanzetta I, Hildesheim R, Grinvald A. 2005. Compartment-resolved imaging of activity-dependent dynamics of cortical blood volume and oximetry. J Neurosci. 25:2233–2244.
Womelsdorf T, Anton-Erxleben K, Pieper F, Treue S. 2006. Dynamic shifts of visual receptive fields in cortical area MT by spatial attention. Nat Neurosci. 9:1156–1160.
Ylinen A, Bragin A, Nadasdy Z, Jando G, Szabo I, Sik A, Buzsaki G. 1995. Sharp wave-associated high-frequency oscillation (200 Hz) in the intact hippocampus: network and intracellular mechanisms. J Neurosci. 15:30–46.